Hindawi
International Journal of Polymer Science
Volume 2023, Article ID 6387898, 21 pages
https://doi.org/10.1155/2023/6387898

Research Article

Investigating the Effect of Curing Activators on the Cure Kinetics of Acrylonitrile–Butadiene Rubber Filled with Graphene Oxide and Reduced Graphene Oxides Nanocomposites

Bismark Mensah,[1] **Boateng Onwona-Agyeman**,[1] **Johnson Kwame Efavi**,[1] **Ralph Abakah Ofor**,[1] **Mawufemor Zigah**,[1] **Joyce Koranteng**,[1] **Maxwell Karikari**,[1] **Frank Nsaful**,[2] **and Daniel Akwei Addo**[3]

[1]*Department of Materials Science and Engineering, CBAS, University of Ghana, Legon, Ghana*
[2]*Department of Food Processing and Engineering, CBAS, University of Ghana, Legon, Ghana*
[3]*Department of Computer Engineering, KNUST, Kumasi, Ghana*

Correspondence should be addressed to Bismark Mensah; bismarkmensah@ug.edu.gh

Received 23 September 2022; Revised 15 March 2023; Accepted 20 March 2023; Published 6 April 2023

Academic Editor: Khubab Shaker

For the first time, acrylonitrile–butadiene rubber (NBR)–graphene oxide (GO) and reduced graphene oxide (rGO) composites were prepared without cure activators: zinc oxide/stearic acid (ZnO/SA) and studied. The vulcanization characteristics of the compounds were systematically studied at 160–190°C, with the aid of rheometer and differential scanning calorimetry (DSC) techniques. NBR revealed rapid curing time (t_{90}) with greater cure rate index compared with NBR–GO/rGO composites for the rheometer measurement. This results were in correspondence with the activation energies E_a (kJ/mol) calculated by Ozawa and Kissinger models of vulcanization kinetics. NBR–rGO obtained reduced t_{90} and E_a (kJ/mol) than NBR–GO, perhaps due to lower oxygenated groups: epoxide (–C–O–C–), carboxyl (–O–C=O), and hydroxyl (–OH) present. Although, the composites delayed in curing, they significantly recorded high tensile properties with high reinforcing factors than NBR. The order of increasing mechanical properties: NBR < NBR–rGO < NBR–GO followed the same order of increasing crosslinking density. In terms of tensile strength, NBR–GO-1 obtained 62.5% and 18.2% increment than NBR and NBR–rGO-1, respectively. The findings from this study indicate that the absence of ZnO/SA in rubber compounds may slow down curing of rubber–GO/rGO composites and lower networks compared with those containing activators ZnO/SA. However, optimization of ZnO/SA and with desired functional groups on graphene and derivative graphene sheets (GDS) including other proposed factors may enhance the curing speed of rubber–GDS based systems, without compromising their mechanical integrity for advanced applications.

1. Introduction

Experts in polymer nano-science and those skilled in the art of rubber processing technology are making determinations to tailor rubber matrices to acquire at least one of the exclusive multifunctional properties of the two-dimensional graphene/derivative graphene sheets (GDS), which include excellent thermal conductivity of ~5000 W/(m K), ultimate strength of ~130 GPa, and a very high electrical conductivity of ~6000 S/cm[12]. Another reason is that, only small amount ~0.05 parts per hundred of rubber (phr) of GDS is used to achieve the same reinforcement effect obtained by concentrations ≥~5 phr of carbon blacks (CB), nanoclays (NC), and silica [1–10]. The tailoring involves synergy formation between the matrix and GDS by using processing techniques like spraying/coting of polymers with GDS [11], melt processing, solvent intercalation [1, 12], and in situ polymerization [1, 13] for advanced applications [1, 7, 14]. Remarkable applications including heat resistance [15–17], sensors [12, 18, 19], electromagnet shields [20], quantum dot materials

[21], damping isolation bearings [22], and high strength uses [1, 7] have been reported.

In rubber–GDS compounding, standard ingredients, such as curing agent (sulfur or peroxides) [23–26], accelerator from the following: dithiocarbamate, thiuram, thiourea, isopropylxanthate, and 2-mercaptobenzothiazole have been used [27–30]. The metallic zinc oxide (ZnO) is one of the common activator incorporated alongside with co-activator like stearic acid (SA) [23–26] for enhancing the vulcanization rate and the efficiency [8, 31]. The ZnO forms zinc stearate, which activates the action of the accelerator system to increase the efficiency of vulcanization [23–26]. In the end, infinite crosslinks/network structures are formed as a result of the reactions among the sulfurating species and with the saturated (–C=C–) sites of the rubber matrix [9, 10, 32].

The vulcanization of rubber–GDS is therefore crucial, since it determines the overall performance and the price of the end product [10, 23–26]. Rubber–GDS composites vulcanization have generated an ongoing debate, as to whether GDS delays or shortens the time for vulcanizing a virgin rubber matrix. The delay is a measure of higher values recorded for the on-set of curing time (t_{s1}, t_{s2}, or t_{s5}) and the optimum curing time (t_{90} and t_{95}) [1, 8, 32–34] deduced from rheo-curves [1, 9, 10, 33, 35, 36]. The changes in curing times with respect to the torque can further be computed into activation energies (kJ/mol) by using popular kinetic models like that of Kissinger [37] and Ozawa [38].

Earlier, Varghese et al. [39] reported that GDS adsorb the curatives in the NBR–GDS composite and hence delayed curing of NBR, just as NC and nanotubes adsorbed curatives in rubber matrices [12, 40, 41]. In addition, Azizli et al. [42], recently linked delays in curing carboxylated (NBR)/ethylene propylene diene monomer (EPDM) rubber blend–GDS composites to the adsorption of the curatives by the GDS present. In terms of filler content, the work of Wu et al. [33], reported that ≤~ 3 phr of graphene accelerated curing of natural rubber (NR) but >~3 phr of graphene delayed curing of NR. Further explanation was made by Allahbakhsh et al. [43], who suggested that proper dispersion of GDS in rubber matrix leads to faster curing in rubber–GDS composites. Other reports still emphasize that the speed of curing of rubber–GDS is dependent on the high surface area of the sheets [1, 7]. Yet, it was proposed that instead of adsorption/absorption of the curatives, the GDS rather participate in the vulcanization process by reacting with the activators/accelerators, with the curing agent (sulfur) and with the rubber matrix [33, 44]. This process confines the rubber chains, resulting in delaying the diffusion of the curatives to complete curing of the matrix.

Mensah et al. [44, 45] further observed that differences in functional group (–C–O–C–), carboxyl (–O–C=O), and hydroxyl (–OH), on GDS (GO and rGO) and the difference in the chemistry of the cure ingredients (curing agent, accelerator, and activator), may greatly influence the overall curing of rubber–GDS composites. To verify whether the absence of accelerators or activators would delay or increase cure reactions, in relation to physico-mechanical properties of the compounds, Mensah et al. [32], initially prepared NBR–GO compounds with sulfur accelerating components without tetramethylthiuram disulfide (TMTD), and the results confirmed that curing was strongly dependent on the oxygen–carbon ratio of GDS.

The present study further cross-examines the effect of removing the cure activator (ZnO/SA) from NBR–GO/rGO composites. Samples were prepared with combined method of solution and melt mixing. Vulcanization tests were done using cure rheometer and differential scanning calorimetry (DSC) techniques. The cure and other properties of NBR–GO/rGO without ZnO/SA were compared with representative samples of NBR–graphite (GRT), those containing all the curing ingredients [44, 45] and those prepared without TMTD [32]. The findings provide insights on controlling the curing speed of rubber–GDS composites with the cure ingredients, without compromising their mechanical integrity for future applications.

2. Experimental

2.1. Chemicals and Compound Formulation. Acrylonitrile–butadiene rubber (NBR, KNB 25LM™, acrylonitrile content: 20–30%, was provided by Kumho Petrochemical Company, Seoul, Korea. The curatives: sulfur (S), TMTD, and *N*-cyclohexyl-2-benzothiazolysulfenamide (CZ) were all acquired from Intelligent Polymer Nano Lab, Polymer Nanotechnology Department, Jeonbuk National University (Jeonju, South Korea). The natural GRT flakes and the other reagents (NH_4OH and hydrazine solutions) were procured from Sigma–Aldrich (St. Louis, MO, USA). The graphene oxide (GO) and reduced graphene (rGO) nanosheets were synthesized by Hummer's method and characterized following the same method as previously reported by Mensah et al. [45]. The pH of the synthesized GO nanosheets was ~5.0, whereas that of the rGO nanosheets range from ~6 to 8 upon the intensive reduction by using NH_4OH and hydrazine solutions. The GO and rGO used in this work had a thickness within ~0.83–2 nm and hydrodynamic size within 100–120 nm [32]. Table 1 shows the compound design expressed as phr.

2.2. Compounding of NBR–GO/rGO/GTR Composites. The NBR rubber was chopped into bits and dissolved in acetone after magnetic stirring for approximately 12 hours at 45°C. The fillers (GO, rGO, or GRT) were homogeneously distributed in dimethylformamide solution by ultrasonication for ~2 hours and subsequently mixed with the NBR rubber solution. The NBR–GO/rGO/GRT mixtures were mechanically stirred using magnetic stirrer at 60°C for about 12 hours until homogeneous solutions were observed. De-ionized water was then added gradually to the homogeneous mixtures of NBR–GO/rGO/GRT rubbers while stirring with a spatula in order to prevent rapid phase separations between GO/rGO or GRT and the NBR matrix. The amalgamated NBR–GO, NBR–rGO, or NBR–GRT rubber nanocomposites were collected from the solution. The amalgamated samples were dried in hot air oven at 80°C until they were moisture free. Later, an estimated amount of standard sulfur curing additives were gradually added, and the compound was passed over a two-roll mill (Model: DS-1500R, Withlab

Table 1: The compositions without ZnO/SA and compounds with reduced activators.

Code/ingredient	NBR	ZnO	CZ	SA	TMTD	S	GO/rGO/GRT
NBR	100	—	0.5	—	0.25	2	0
NBR–GRT-1	100	—	0.5	—	0.25	2	1
NBR–GO-0.1	100	—	0.5	—	0.25	2	0.1
NBR–GO-1	100	—	0.5	—	0.25	2	1
NBR–rGO-0.1	100	—	0.5	—	0.25	2	0.1
NBR–rGO-1	100	—	0.5	—	0.25	2	1
Case study: compounds with reduced ZnO/SA ratio (1 : 1)							
NBR	100	1	0.5	1	0.25	2	0
NBR–GRT-1	100	1	0.5	1	0.25	2	1
NBR–GO-1	100	1	0.5	1	0.25	2	1

phr*, parts per hundred of rubber; TMTD, tetramethylthiuram disulfide; CZ, *N*-cyclohexyl-2-benzothiazolysulfenamide; S, sulfur; NBR, acrylonitrile–butadiene rubber; SA, stearic acid, GDS, graphene and derivative graphene sheets, GRT, natural graphite; rGO, reduced graphene oxide graphene; GO, graphene oxide.

Co. Ltd., Seoul, South Korea) for about ~9 minutes, for homogeneous mixing. The samples were then sheeted from two-roll. Sheets of the rubber nanocomposites were cured with a cure rheometer to obtain the curing information at different temperature ranges of 160–190°C. Later, an optimized temperature of 160°C was selected and used to vulcanize the samples in a 15 cm × 15 cm × 2 mm metallic mold using a hot press machine (Caver WMV50H, USA) at a pressure of ~11 MPa. At the end, the cured composite sheets were designed into standard shapes to perform mechanical and other tests for their characterizations.

3. Characterizations

3.1. Scanning Electron Microscopy Analysis. How the graphene sheets (GO and rGO) are dispersed within the typical samples of vulcanized NBR systems compounded devoid of ZnO/SA were examined using scanning electron microscopy (SEM) technique, after the samples were cryogenically fractured. The compounds were later platinum coated via sputtering to reduce the surface resistance at the surface for observing. The surface morphologies were studied with field emission SEM (JEOL, JSM 599, Tokyo, Japan) for ~20 minutes.

3.2. Vulcanization Properties and Kinetics by ODR. A cure rheometer analysis using (oscillating disc rheometer, ODR) was performed on the non-activated samples to ascertain the cure properties at temperatures ranges of 160°C, 170°C, 180°C, and 190°C. The cure characteristics: scorch time (t_{s2}), optimum curing time (t_{90}), cure rate index (CRI), and the torque properties: M_L, M_H, $\Delta M(M_H - M_L)$ were determined from the rheo-curves and studied.

3.2.1. Vulcanization Kinetics by Autocatalytic Model. The cure kinetics of NBR–graphene toughened with plastic were studied by using different kinetic models like Isayev, modified Isayev, Kamal and Ryan, autocatalytic, and model-free approach by Barghamadi et al. [46], In this work, only autocatalytic models (Ozawa and Kissinger) were employed to study the cure kinetics of un-activated NBR–GO/rGO composites in comparison with NBR–GO/rGO without activators and those containing all cure ingredients, which were also studied with the same models earlier reported by Mensah et al. [32, 44]. In this case, the extend of curing (α), rate of curing ($d\alpha/dt$), and activation energy for curing of the various compounds were computed from the rheometer behaviors (torque and cure time).

The standard differential model equation for rubber vulcanization reaction is usually written as Equation (1) [47].

$$\frac{d\alpha}{dt} = k(T)f(\alpha), \tag{1}$$

where $d\alpha/dt$ is the vulcanization rate, t is the time, $k(T)$ is the specific rate constant at temperature T, and $f(\alpha)$ is the function corresponding to the phenomenological kinetic model. The degree of crosslinking, α, given by Equation (2), was determined from the rheometer study [41, 48].

$$\alpha = \frac{M_t - M_0}{M_\infty - M_0}, \tag{2}$$

where M_0, M_t, and M_∞ are the torque values at the time zero, at a given time t of curing, and at the end of crosslinking, respectively. The function $k(T)$ in Equation (1) is related to the activation energy (E_a) by the Arrhenius Equation (3).

$$k(T) = k_0 e^{-E_{a/RT}}, \tag{3}$$

where k_0 is a pre-exponential factor, E_a is the activation energy, and $R(8.314\,\mathrm{J\,mol^{-1}\,K^{-1}})$ is the universal gas constant. The nth order kinetics of chemical reaction, $f(\alpha)$is based on the Borchardt and Daniels, given by Equation (4) [49].

$$f(\alpha) = (1-\alpha)^n, \tag{4}$$

where n is the order of reaction. For a multi-step curing reaction, such as the vulcanization reactions in this current study, Equation (4) can now be written as

$$f(\alpha) = \alpha^m(1-\alpha)^n, \tag{5}$$

where $m$and n are both orders of reaction. Fitting Equation (5) into Equation (1) will yield the vulcanization kinetics for an autocatalytic reaction used in our study.

$$\frac{d\alpha}{dt} = k(T)\alpha^m(1-\alpha)^n. \tag{6}$$

3.3. Vulcanization Kinetics Study by DSC. The non-activated samples were cured using the same differential scanning calorimetry thermal gravimetric analysis (TA Instrument,

SDT Q600 V20.9 Build 20, USA) device. Nitrogen atmosphere, equilibrium temperature of 30°C to maximum of 200°C at different heating rates of 2, 5, 10, and 15°C/min were used. With the help of the DSC curves obtained at the different heating rates, the activation energy (E_a) in kJ/mol of vulcanization reactions in the samples under non-isothermal condition were determine by using Ozawa model [38] in Equation (7).

$$-\frac{E_a}{R} = \frac{d\left[\log\left(\beta\right)\right]}{d\left(1/T_v\right)}, \tag{7}$$

where R is the universal gas constant, β is the heating rate, and T_v is the temperature of vulcanization. Two peaks are mostly observed in exothermic curing peak in DSC curve. One is T_{vi} corresponding to the minimum temperature of vulcanization, whereas T_{vf} corresponds to maximum temperature of vulcanization. The E_a (kJ/mol) of the samples was also calculated by using Kissinger method [37] shown in Equation (8).

$$-\frac{E_a}{R} = \frac{d\left[\ln\left(\beta/T_v^2\right)\right]}{d\left(1/T_v\right)}. \tag{8}$$

3.4. Tensile Properties. Tensile properties of non-activated vulcanizates were measured using a (LLOYD Instrument, UK) with a dumbbell shaped specimen in accordance with ASTM D412. The tensile strength (MPa) was calculated using the maximum stress at fracture and the corresponding elongation at break, E_b (%). The test was done at 25°C and at 500 mm/minutes cross-head speed.

3.5. Determination of Young's Modulus. The Young's modulus E (MPa) of nanocomposites at low strains was determined by gradually loading a rectangular strip (5 cm × 1.5 cm × 0.2 cm) of the samples with variable weights until a complete fracture occurred a laboratory based system as seen in Figure 1. A camera was positioned in one place to carefully monitor each strain upon loading. By taking the acceleration due to gravity into consideration, the weights were converted into force (N) and together with the change in lengths; a stress–strain curves were plotted. The Young's modulus was then computed by using initial slope at lower strain (<5%).

Later, using the classical Equation (9), the E was adopted to calculate the total network density (n_t).

$$E = 3n_tRT, \tag{9}$$

where R is the universal gas constant and T is the absolute temperature.

3.6. Crosslinking Density of Non-Activated Compounds by Swelling. The equilibrium swelling of the non-activated samples; NBR and its NBR–GO/rGO/GRT composites was determined by keeping the vulcanized samples in methyl ethyl ketone (MEK) (molar volume of 89.6 mL/mol) for ~72 hours at 25°C temperature. The uptake of

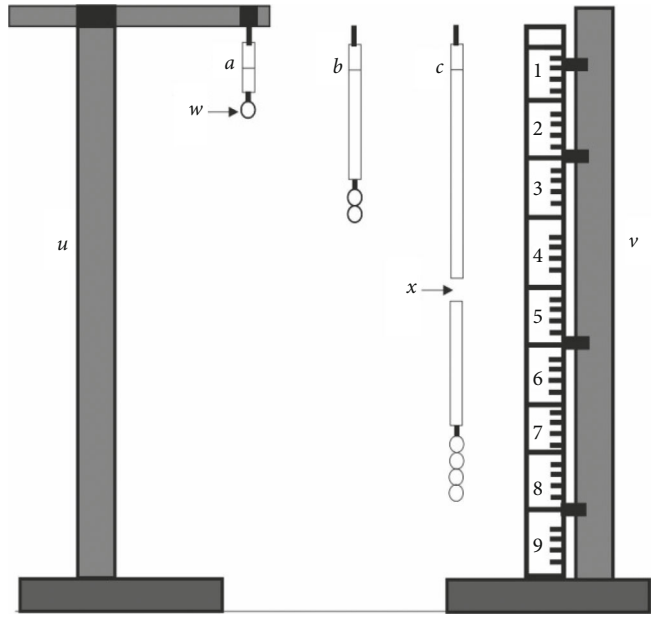

Figure 1: Determination of Young's modulus: (u) fixed support and clamp for the rubber strip, (v) support for the ruler/measuring system, (w) mass load (a, b, and c) rubber strip under different loading level, and (x) point of rubber fracture.

MEK ($W_s - W_i$) and dried weight (W_{dr}) of nanocomposites were used to compute the degree of swelling (Q_r) by using Equation (10).

$$Q_r = \left(W_s - W_i\right)/W_{dr}, \tag{10}$$

where W_i and W_s are the start and finishing weights of nanocomposites before and after swelling. W_{dr} is the dried weight of the nanocomposites. The cross-link density n_c (mol/cm^3) of prepared nanocomposites was calculated by using Flory–Rehner model [50] given by Equation (11).

$$n_c = \frac{-\left[\ln\left(1 - V_2\right) + V_2 + \chi_1 V_2^2\right]}{V_1\left(V_2^{1/3} - V_2/2\right)}, \tag{11}$$

where, v_2 is the volume fraction of NBR in swollen gel at equilibrium. The v_1 is a molar volume of swelling solvent (MEK). The value of interaction parameter (χ_1) between MEK and NBR was found to be ~0.384 on fitting the value of solubility parameters (δ) of NBR (8.9 cal$^{1/2}$/cm$^{-3/2}$) and MEK (9.27 cal$^{1/2}$/cm$^{-3/2}$) in Bristow–Watson relation [51] as given below Equation (11).

$$\chi_1 = \beta_1 + \left(v_1/RT\right)\left(\delta_s - \delta_p\right)^2, \tag{12}$$

where R, T, and β_1 are the universal gas constant (8.314 J/mol K), absolute temperature, and lattice constant (0.34). The δ_s and δ_p are the solubility parameters of MEK and NBR, respectively.

4. Results and Discussion

4.1. Morphology and State of Filler Dispersion in NBR. Previously, transmission electron microscopy (TEM) and atomic force microscopy (AFM) techniques were used to investigate the state of dispersions of NBR–GO and NBR–rGO composites prepared with all the traditional cure ingredients, by Mensah et al. [44, 45]. Presently, SEM technique was adopted to report the state of dispersions of GO and rGO within NBR matrix Figures 2(a), 2(b), and 2(c) are the SEM images for the pure NBR and typical samples: NBR–GO-1 and NBR–rGO-1, respectively, which were prepared without ZnO/SA. As seen in Figures 2(b) and 2(c), it was very difficult to physically observe the dispersions state of the GO or rGO sheets within the cryo-fractured interface of NBR–GO/rGO composites.

This is a common observation for lowly filled nano-sized particles (≥~0.05 phr) like carbon nanotube (CNT) and the flexible graphene sheets (GDS). These particles usually embed themselves deeply within the matrix or get coated by the rubber molecules, thereby making it difficult for SEM observation. Earlier, Nah et al. [52], attempted to resolve this challenge when CNT was incorporated into NR matrix. They had to use a tedious approach to squeeze the lowly filled CNT from the bulk NR to the cryo-fractured surface by compressive strain in the SEM chamber, before it was possible for SEM to clearly show the state of dispersions of the CNTs within the NR.

Challenges in observing dispersions of graphene within NR was also reported by Kang et al. [53]. Furthermore, recent work by Mensah et al. [32, 45] for NBR–GO/rGO compounds without cure co-accelerator and for NBR–GO/rGO compounds containing all the traditional cure ingredients, also reported similar challenges. Unlike the (CNT or GDS) SEM techniques have been very effective tools for studying the morphologies of traditional fillers like CB, fibers (F) [54], and NC incorporated into polymer matrices [55–57]. This is because, for these fillers, high concentrations ≥~5–60 phr are required to achieve effective reinforcement of rubber matrices [55, 56]. Hu et al. [58], resorted to increase the GO content, by forming a blend of GO and halloysite nanotube in order to assist the dispersions and observation of GO in NBR matrix by SEM method.

When compared, some strain induced-cracks at the cryo-fractured interface of the pure NBR (Figure 2(a)) can be seen, even though such effect was not observed for the composites (Figures 2(b) and 2(c)). Instead, strain-induced surface roughness was seen, which was obvious for the NBR–GO-1 compound (Figure 2(c)). The strain-induced surface roughness was reported to be due to stronger filler–rubber chain interactions or tighter structures induced by the successfully dispersed GO or rGO sheets. The GO/rGO sheets promoted physical and chemical interlocking with adjacent rubber chains [1].

While the strain-induced surface roughness effect of the composites is anticipated to have effects on the physico-mechanical properties of the filled compounds, other tests like the rheological properties, equilibrium swelling test, and tensile properties have been presented to investigate the dispersion state of GO and rGO in NBR matrix.

4.2. Reaction Mechanism of Un-Activated Compounds. The mechanism of vulcanization of NBR, NBR–GO, and NBR–rGO containing standard ingredients (TMTD + CZ + ZnO/SA + sulfur) has been explained in detailed in our earlier report [44]. Briefly, during the crosslinking process, accelerator–zinc complexes or covalently bonded polysulfidic–Zn structures (benzothiazyl [BT]–S–S_x–Zn–S–BT) are formed as depicted in Figure 3(a). The BT, is an organic radical resulting from CZ [27, 30]. The ZnO/SA activates the vulcanization process, upon which H_2O is formed to help minimize side reactions in TMTD. The H_2O also behaves as a ligand in the creation of more BT–S–S_x–Zn–S–BT structures [27, 30].

The reaction of BT–S–S_x–Zn–S–BT with the diene sites (–C=C–) of NBR to produce sulfurated NBR (NBR–S_x–S–BT) also occurs. Finally, more NBR–S_x–S–BT react together or with –C=C– to form infinites crosslinks NBR–S_x–S–NBR structures. Secondary reactions by the oxygen rich-GO and rGO occurs between the curing additives and with the rubber matrix, thereby increasing the total network density [44].

In the absence of ZnO/SA (Figure 3(b)), the vulcanization reactions lead to the formation of organic pendant groups (BT–S–S_x–S–BT) with limited amount of zinc complexes produced [33, 45]. Little or no amount of H_2O is produced from the reaction to control the side reactions in TMTD to sustain the vulcanization process. Furthermore, owing to the high thermal conductivity behavior of zinc in the zinc complexes BT–S–S_x–Zn–S–BT, the formation of sulfurating of NBR species (NBR–S_x–S–BT and NBR–S_x–S–NBR) to form infinite crosslinking reactions may be faster than those without zinc complexes (BT–S–S_x–S–BT; Figure 3(b)). Hence, delays in curing of the NBR and NBR–GO/rGO composites without ZnO/SA are expected, and may affect the network density and overall properties of the end material. However, the high thermal conductivity behavior of GO/rGO and the presence of the numerous oxygen moieties, such as epoxide (C–O–C), hydroxyl (–OH), and carboxylic (–O–C=O), may provide self-activation during vulcanization process, in order to reduce the consequences due to the absence of the zinc complexes.

4.3. Vulcanization Behavior of Compounds by Cure Rheometer. The cure characteristics, such as scorch time, t_{s2} (minutes), optimum curing time, t_{90} (minutes), torque properties: minimum torque (M_L), maximum torque (M_H), the difference, $\Delta M(M_H - M_L)$, and the CRI (minutes^{-1}) CRI = $100/(t_{90} - t_{s2})$, which is a measure of the speed of vulcanization reaction were all obtained from rheo-curves and are compared in Table 2. A decreasing trend of t_{s2} and t_{90} values can generally be seen from 160°C to 190°C for all the compositions at 0.1–1 phr of filler loading.

On removal of the ZnO/SA from the composition all the specimen showed different scorch time (t_{s2}) values, with the pure NBR delaying in t_{s2} than the rest. The NBR–rGO-1 displayed a quicker scorch time (t_{s2}) than the NBR–GO-1 and NBR–GRT-1, notably at lower temperatures. When the t_{90} are compared, the samples show closely related values, as seen in Table 2. However, on close examination, especially at lower temperatures, NBR exhibited faster curing behavior

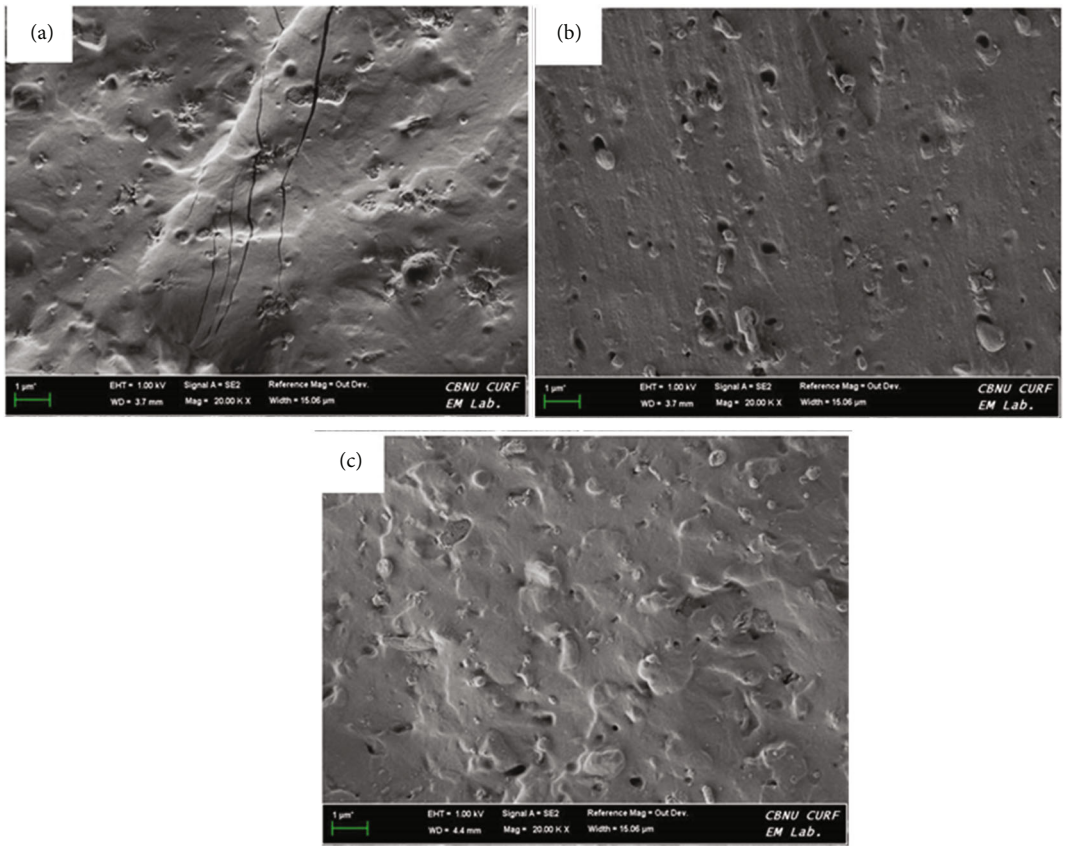

Figure 2: Morphological properties of compounds by SEM analysis: (a) NBR. (b) NBR–rGO-1. (c) NBR–GO-1.

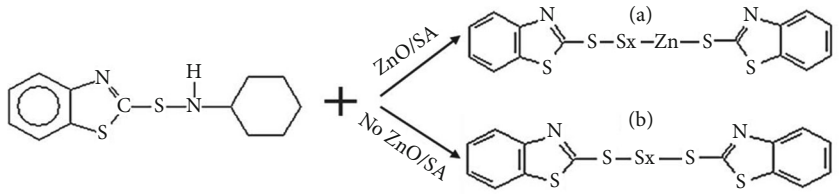

Figure 3: Typical reaction mechanism of non-activated cure systems. (a) Curing reactions of compounds containing activator systems and (b) curing reactions of compound without activator systems.

than rest of the samples. At lower filler loading (0.1 phr) the curing of NBR was faster for NBR–GO-0.1 than NBR–rGO-0.1, but on increasing the filler to 1 phr, the reverse occurred, as NBR–rGO-1 obtained relatively shorter t_{90} values. This observation may be due to GO aggregation or the delay caused by the participation of the high oxygen moieties during curing reactions.

Interestingly, the NBR–GRT-1 showed higher t_{s2} and t_{90} values when compared with the oxygenated counterparts (GO and rGO). In addition, an increasing trend for the CRI can be seen from 160°C to 190°C, for the compositions and at all filler loadings; the sequence of decreasing CRI for the highly loaded compounds is NBR > NBR–rGO-1 > NBR–GO-1 > NBR–GRT-1, as shown in Table 2. Thus, it can be establish that, the absence of oxygen groups on GRT does not favor the curing of NBR, whereas higher oxygen content may still delay the curing of NBR.

Generally, the decreasing order of oxygen (O)/carbon (C) ratio for GDS is GO > rGO > GRT as already reported [45]. The order suggests that O/C ratio is very critical in the curing rubber–GDS based composites. The faster curing behavior of the pure matrix (NBR) may be due to diene structures (–C=C–), which are readily attacked by polysulfidic species and converted into crosslinks. Only primary crosslinking reactions may occurs in NBR; however, a series of secondary crosslinking reactions between the NBR and GO/rGO/GRT occurs in addition to the primary crosslinking reactions before reaching matured vulcanization state. The overall consequence is the delay in curing of the composites [44].

In comparison, the current result contradicts those presented by Raef et al. [59], who reported the cure rate (CRI) of SBR–GO composite to be higher than that of SBR–rGO composites, prepared via latex compounding, irrespective of the lower bound observed for SBR–GO than SBR–rGO.

Table 2: Cure properties of non-activated sulfur cured NBR systems.

Compounds	T (°C)	M_H (dNm)	M_L (dNm)	ΔM (dNm)	t_{90} (minutes)	t_{S2} (minutes)	CRI
NBR	160	33.01	3.18	29.83	29.36	2.76	3.76
	170	32.36	3.04	29.32	14.94	1.82	7.62
	180	31.78	2.93	28.85	8.36	1.41	14.39
	190	31.87	3.02	28.85	5.35	1.11	23.60
NBR–GRT-1	160	34.28	3.29	30.00	30.56	2.23	3.53
	170	33.80	3.28	29.88	21.13	2.05	5.24
	180	33.32	3.26	29.76	13.15	1.58	8.64
	190	32.89	3.25	29.64	5.60	1.12	22.32
NBR–GO-0.1	160	35.05	4.04	31.01	29.19	2.56	3.76
	170	34.56	3.89	30.67	14.09	1.82	8.15
	180	33.84	3.59	30.25	7.70	1.38	15.82
	190	33.98	3.49	30.49	4.99	1.12	25.84
NBR–GO-1	160	35.15	4.00	31.15	30.97	2.85	3.60
	170	34.95	3.93	31.02	15.33	2.03	7.52
	180	32.77	3.57	29.20	8.51	1.32	13.90
	190	30.59	3.60	26.99	5.69	1.25	22.50
NBR–rGO-0.1	160	34.43	3.96	30.47	30.00	2.77	3.67
	170	33.74	3.89	29.85	15.07	2.11	7.72
	180	33.22	3.77	29.45	8.67	1.69	14.33
	190	32.84	3.56	29.28	5.81	1.41	22.74
NBR–rGO-1	160	35.10	3.61	31.49	30.16	2.74	3.65
	170	33.86	3.50	30.36	14.38	1.93	8.03
	180	33.25	3.42	29.83	8.40	1.45	14.40
	190	33.11	3.27	29.84	5.58	1.23	23.00

The t_{s2} and t_{90} were extremely longer with corresponding lower CRI compared with the compounds (NBR, NBR–GO, and NBR–rGO), which contained ZnO/SA and TMTD reported by Mensah et al. [44] and those without TMTD accelerator by Mensah et al. [32]. However, it is interesting to observe that the t_{s2} and t_{90} of the current work are relatively lower compared with those obtained for SBR–rGO and SBR–GO composites prepared by latex compounding technique by Raef et al. [59], which contained ZnO/SA. For instances, SBR–GO-1 and SBR–rGO-1 recorded 7.91 and 8.91 minutes for the t_{s2}, respectively. Similarly, polar NBR was found to cure faster than non-polar matrix like EPDM, reinforced with GO and rGO particles [8, 35]. These observations suggests that although cure ingredients may greatly influence the curing properties of rubber–GDS composites; however, the choice of processing technique and matrix used may also affect the final vulcanization properties of rubber–GDS compounds.

Meanwhile, when NBR matrix was incorporated separately with GO, rGO, and even GRT in the absence of ZnO/SA, the viscosity index (M_L), mechanical strength index (M_H), and the crosslinking density index (ΔM) for the composites got relatively higher compared with the virgin gum (NBR). Typically, the order of the increasing in M_H property is: NBR–GO > NBR–rGO > NBR–GRT > NBR. This order may be due to the reinforcing actions offered by these fillers [1].

4.3.1. Vulcanization Behavior Based on Autocatalytic Model. The graphs of the degree of conversion (α) per cure time (minutes) for the representative samples are shown in Figure 4(a), whereas the $d\alpha/dt$ per time (minutes) for the NBR and the highly filled samples are shown in Figure 4(b). In Figure 4(a), NBR generally reaches full conversion (α) in shortest time interval compared with the highly filled samples (NBR–GO-1 and NBR–rGO-1), clearly seen at lower temperatures.

In addition, the maximum $d\alpha/dt$ for the NBR shifts towards shorter time while that of the composites moves towards longer curing times as seen in Figure 4(b). The graph of $(d\alpha/dt)$ against α for NBR and the NBR–GO-1 at 160–190°C is shown in Figures 4(c) and 4(d). The solid lines represent the theoretical fitting curves obtained from a nonlinear regression plot. As seen, there is a close correlation between the experimental data and the theoretical fitting with strong correlation coefficient of $R^2 \sim 0.99$ for all the curing temperatures and for all the samples. A common trend can be observed, there is a lower rate of conversion at lower temperature, whereas higher temperatures result in higher rate of conversion (Figures 4(c) and 4(d)).

The lower $d\alpha/dt$ observed at lower temperatures can be attributed to increased viscosity of the compounds, which impeded the creation of crosslinks between neighboring polymer chains, as earlier observed by Kader and Nah group [60].

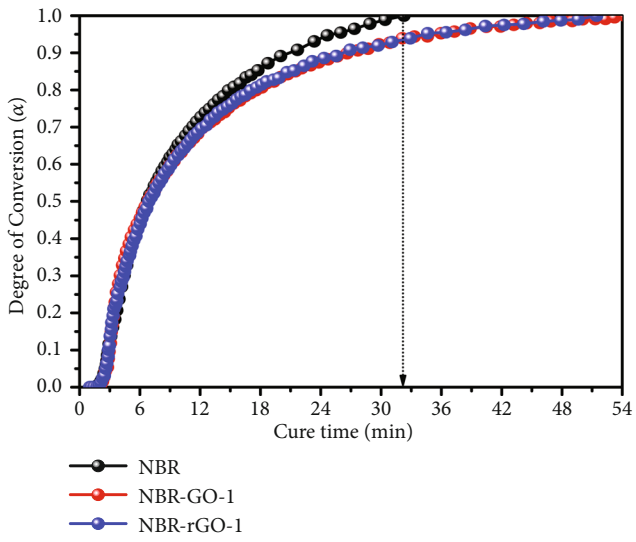

(a)

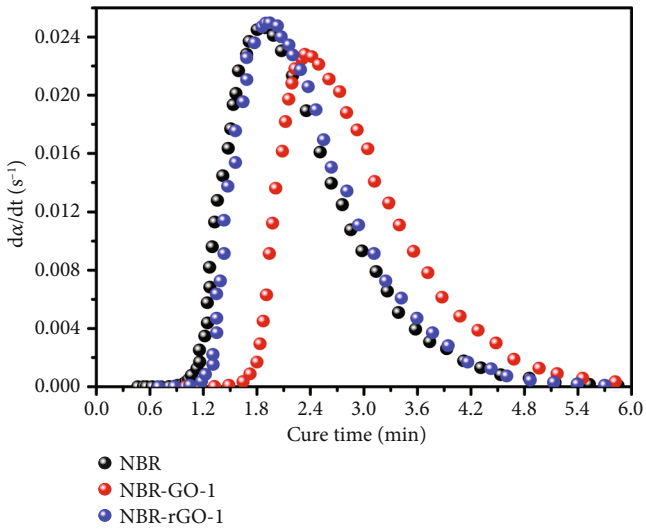

(b)

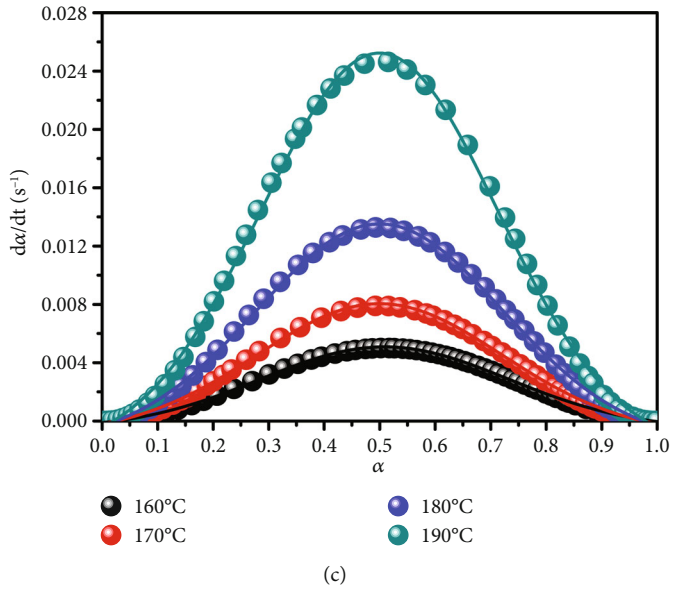

(c)

Figure 4: Continued.

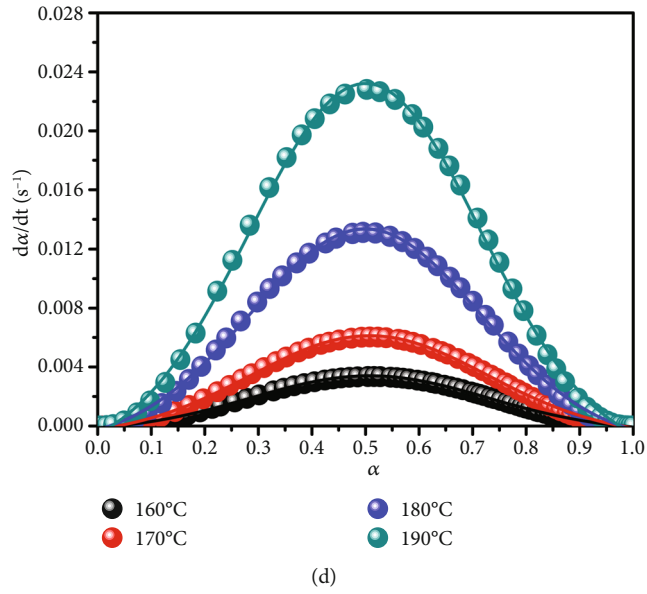

Figure 4: The autocatalytic properties of the compositions: (a) cure rate of conversion (dα/dt) as a function of (b) dα/dt at cure time (minutes), (c) dα/dt versus the conversion (α) for NBR at160°C–190°C, and (d) dα/dt versus the conversion (α) for NBR–GO-1 at 160–190°C.

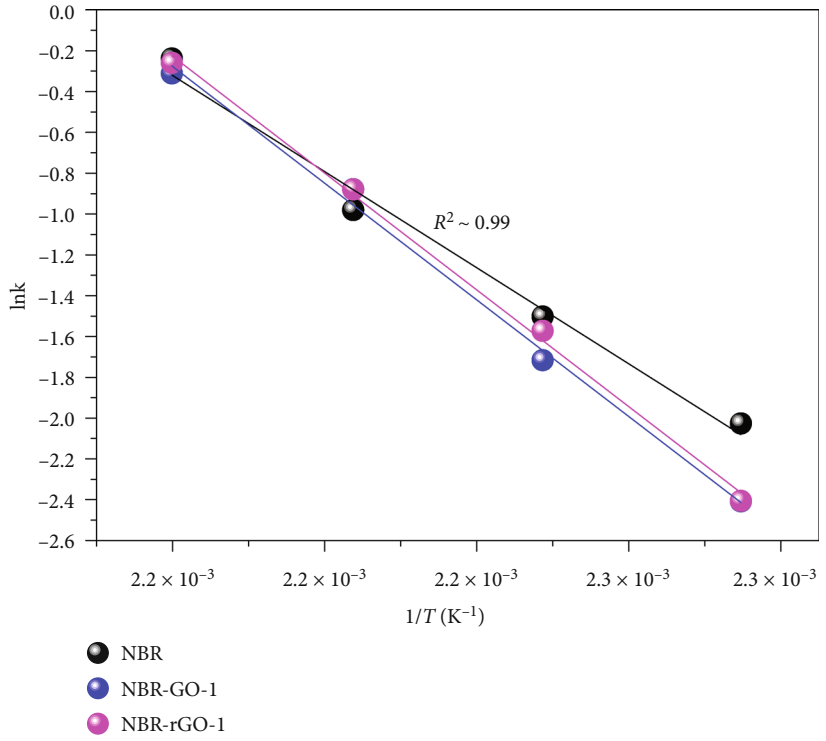

Figure 5: Arrhenius plot of ln$k$ versus 1/T for non-activated NBR, NBR–GO, and NBR–rGO nanocomposites.

As temperature increased, drop in viscosity and chain mobility of the rubber molecules occurred. Rapid melting of the sulfurating species also occurred; this ultimately resulted in an increase in the rate of conversion. The NBR showed relatively higher conversion (α) and dα/dt behavior as compared with the composites. This may be due to the readiness of the dienes (–C=C–) in its structure to form crosslinks (C–S_x–C and C–S–S_x–C) with polysulfidic species, as temperature increases. On the other hand, the composites are expected to show higher network density (tight structures or restrained mobility) than NBR after conversion, especially at optimized curing temperature (160°C), due to the additional networks introduced by the incorporated GO and rGO sheets[10, 32].

Table 3: Cure kinetic parameters of un-activation sulfur cured NBR, NBR–rGO, and NBR–GO systems.

Compounds	T (°C)	k	m	n	$m+n$	k/t_{90}	E_a (kJ mol^{-1})
NBR	160	0.13	2.4	2.3	4.7	0.004	97.91 ($R^2 \sim 0.98$)
	170	0.22	2.4	2.4	4.8	0.015	
	180	0.37	2.4	2.4	4.8	0.004	
	190	0.79	2.5	2.5	5.0	0.15	
NBR–GO-1	160	0.10	2.5	2.4	4.9	0.003	118.90 ($R^2 \sim 0.99$)
	170	0.18	2.5	2.4	4.9	0.012	
	180	0.42	2.5	2.5	5.0	0.051	
	190	0.73	2.5	2.5	5.0	0.13	
NBR–rGO-1	160	0.10	2.5	2.50	5.0	0.003	118.95 ($R^2 \sim 0.99$)
	170	0.21	2.5	2.53	5.3	0.015	
	180	0.41	2.5	2.50	5.0	0.05	
	190	0.77	2.5	2.50	5.0	0.13	

The slope of the Arrhenius plots shown in Figure 5 based on Equation (11) was used to determine the E_a (kJ/mol) of cure reactions, which is related to the ease of crosslinking reaction. The experimental findings fit with hypothetical predictions, showing high correlation coefficient ($R^2 \sim 0.99$).

In addition, the kinetic factors; (E_a, n, m, and k) of the autocatalytic reactions of the non-activated compounds are shown in Table 3. The total reaction order ($m + n$) is seen increasing slightly compared with that of the gum, as temperature progressed. The change in the reaction order ($m + n$) is an evidence that GO/rGO sheets participate in the curing reactions [33]. The rate constant (k) shows an inverse relationship with the t_{90}, but direct relations with the CRI as temperature increases. A comparable observation was stated by Choi et al. [26], for NBR-organo-modified clays and NR–CNT by Sui et al. [61] by autocatalytic modeling of cure kinetics.

The composites generally required higher E_a (kJ/mol) for the autocatalytic curing reactions than the virgin NBR. The NBR–GO and NBR–GO sample exhibited comparable E_a (kJ/mol) values of (118.90 kJ/mol) and (118.95 kJ/mol), respectively. This result is generally in accordance with the rheometric properties (t_{s2} and t_{90}) shown in Table 2.

4.4. Vulcanization Kinetics by DSC Method. For better understanding, the DSC method was used to examine the curing characteristics of the non-activated sulfur cured NBR, NBR–rGO, and NBR–GO systems by considering the changes in heat flow rate during curing reactions [33]. The exothermal peaks, which are shown in Figure 6, are the minimum (T_{iv}), maximum vulcanization (T_{fv}) temperatures, and the melting temperature (T_m). These notable temperatures have been utilized to estimate the E_a (kJ/mol) [32].

Presently, T_{iv} and T_{fv} were used to calculate the E_a (kJ/mol) values according to Ozawa method in Equation (7) and Kissinger model in Equation (8) [37]. A representative DSC cures curves for un-activated compounds; NBR, NBR–rGO-1, and NBR–GO-1 at 15°C/minutes heating rate have been shown in in Figure 6. From the curves, T_{iv} shifted to lower temperatures, whereas the T_{fv} shifted towards higher temperatures. By considering the positions of the exothermic peaks (T_{iv} and T_{fv}), the crosslinking of NBR was first achieved at lower temperatures, whereas those of the composites were realized at higher vulcanization temperatures with prolonged times.

The representation of the plots of lnβ against $1000/T_{iv}$ based on Ozawa approach is shown in Figure 7(a) and that of Kissinger model is shown as plot of ln (β/T_{vf}) versus $1000/T_{fv}$ in Figure 7(b). A strong correlation ($R^2 \sim 0.99$) between the experimental and theoretical data was observed Figures 7(a) and 7(b).

The slopes, activation energy E_a (kJ/mol) obtained from the plots in Figures 7(a) and 7(b) are compared in Table 4 for the case of Ozawa and Kissinger models. The increasing order for the E_a (kJ/mol), particularly those deduced at the maximum vulcanization (T_{fv}) temperatures: NBR > NBR–rGO-1 > NBR–GO-1. This observation is somewhat in agreement with the rheometer curing properties (Table 2). The reason for this observation is that, initially the physical presence of the GO and rGO confined the molecular chains of NBR and hence delayed melting and diffusion of curatives to start vulcanization [33, 44].

In addition, during the vulcanization process, the oxygenated functionalities; epoxide (–C–O–C–), carboxyl (–O–C=O), and hydroxyl (–OH) on GO/rGO are noted to partake in the crosslinking reaction with the polysulfidic groups, the NBR matrix, and even among themselves [33, 44] to form tighter networks structures, such as NBR–S_x–GO–S–NBR and NBR–S_x–rGO–S–NBR [44].

These secondary crosslinking reactions by the GO/rGO and the initial stiffening of NBR matrix, elevated the E_a (kJ/mol) barrier, and therefore extended the vulcanization periods for the filled compounds, as compared with the pure NBR.

NBR–rGO exhibited lower E_a (kJ/mol) than NBR–GO-1 possibly due to the higher oxygenated groups (O/C ratio) on GO sheets, as these functionalities may have higher reactivity with the curatives, and therefore could raise the E_a (kJ/mol) barrier for vulcanization [1, 33, 44]. By comparison, the E_a (kJ/mol) achieved in these present samples are relatively greater compared with NBR, NBR–rGO, and NBR–GO compounded with ZnO/SA and TMTD, reported by

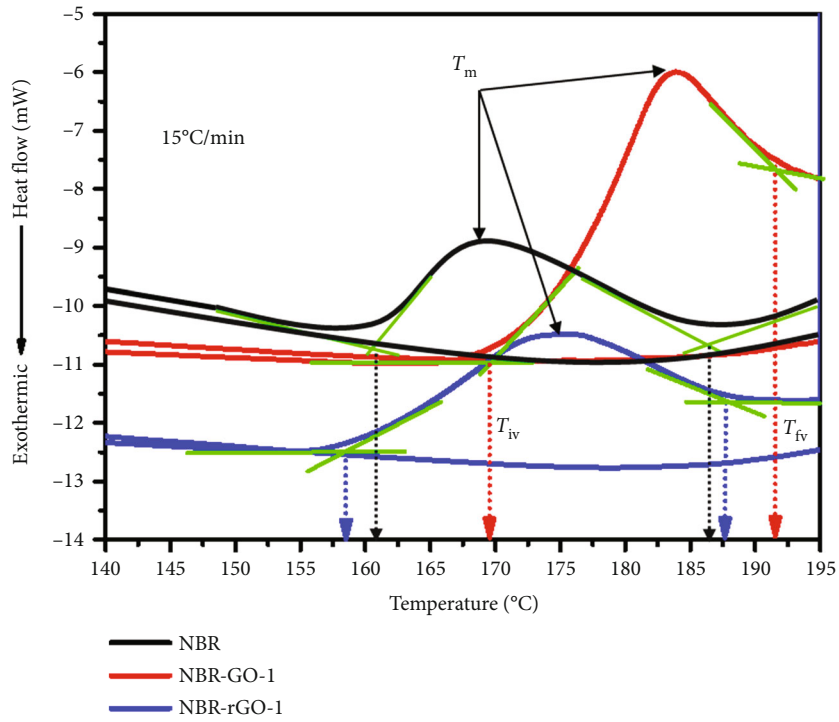

Figure 6: A typical DSC curve obtained for the non-activated sulfur cured vulcanizates at 15°C/minutes heating rate.

Mensah et al. [44]. This current study opposed the observation that GO lowers E_a (kJ/mol) barrier for curing SBR compared with rGO, due to high immobilization of bound rubber content in SBR–rGO composites [59].

4.4.1. Vulcanization Behavior of Optimized Compounds. In order to verify the role of the ZnO/SA on the vulcanization behavior of NBR, in the presence and absence of oxygenated groups on graphene, typical samples of NBR–GO-1, NBR, and NBR–GRT-1, were prepared with 1 phr of ZnO and 1 phr of SA. The optimum cure time (t_{90}) and CRI are shown in Figures 8(a) and 8(b). It is interesting to observe that, GO (highly decorated with high oxygen groups) now showed relatively lower t_{90} with corresponding higher CRI than NBR. With NBR–GRT showing delays with lower CRI behavior.

Therefore, it can be suggested that the oxygenated groups: epoxide (–C–O–C–), carboxyl (–O–C=O), and hydroxyl (–OH) decorating the graphene sheets, do not only participate in the crosslinking process of NBR, but these moieties also determine the speed of the crosslinking reactions. However, this will strongly depend on the ratios of the activator (ZnO/SA) and accelerator (TMTD/CZ) [33] incorporated in the design.

4.5. Effect of Vulcanization on Physico-Mechanical Properties

4.5.1. Viscosity and Strength Index. The minimum torque (M_L) and the strength index (M_H) for the non-activated vulcanized NBR compounds reinforced with GO/rGO and GRT at high filler concentration are shown in Figures 9(a) and 9(b), respectively. General trend can be seen, the M_L for filled and unfilled compounds dropped as temperature proceeded from 160°C to 190°C. The composites showed relatively higher M_L properties than NBR, especially at low graphene loading (0.1 phr). A similar trend was seen for the highly filled compounds, the trend of increasing M_L is given by: NBR < NBR–GRT < NBR–rGO < NBR–GO. Among the composites, NBR–GO showed higher M_L values, especially at higher filler loading. The M_L for the present compounds are lower compared with those prepared in the presence of ZnO/SA [44].

Again, the composites showed higher M_H values compared with the neat NBR at all filler loading levels (0.1–1 phr) and the order of increasing M_H for both lowly and highly filled compounds, especially at lower temperatures is: NBR < NBR–rGO < NBR–GO and NBR < NBR < NBR–GRT < NBR–rGO < NBR–GO, respectively. The increment in M_L and M_H for the composites, with NBR–GO leading may be as a result of the stiffer network structures, such as NBR–S_x–GO–S_x–NBR and NBR–S_x–rGO–S_x–NBR and the large number of polar–polar interactions (–$CN^{\sigma-}$–$H^{\sigma+}$–O–) between the rich oxygenated groups (–OH) of GO/rGO and CN of NBR [44, 62]. The NBR–GO composites showed the highest properties due to the high O/C ratio of GO than rGO and GRT.

However, the high M_L value of NBR–GRT-1 compared with NBR may only be due to physical restraints of the flexibility of the rubber molecules by the physical presence of the GRT sheets, as proposed by Einstein and Guths–Gold viscosity theory [1, 63]. An interesting observation can be seen at higher temperatures, that is, the M_L and M_H of the compounds seem to drop from 170°C to 190°C. The sharp drop behavior may be due to due thermal oxidative

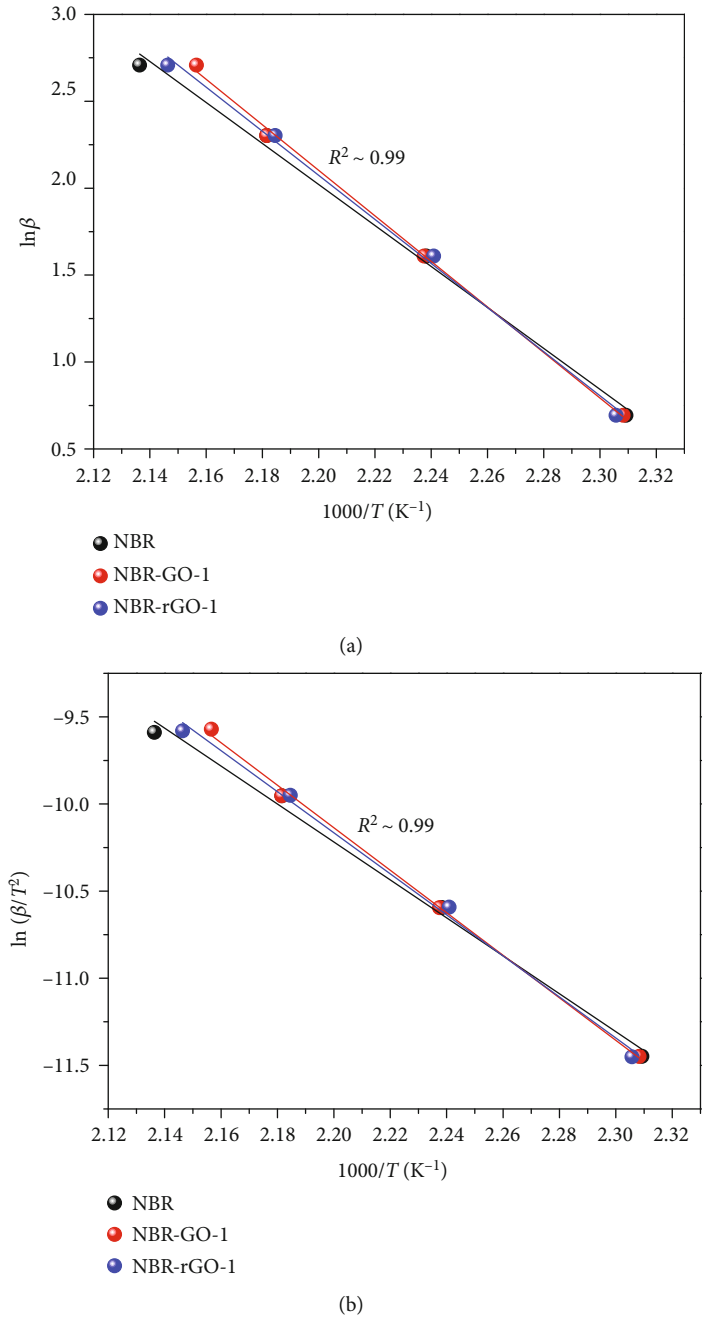

Figure 7: The Ozawa (a) $\ln\beta$ versus $1000/T$, and Kissinger (b) $\ln(\beta/T^2)$ versus $100/T$ plots for the determination of energy of activation (E_a) for curing of non-activated NBR and its nanocomposites (NBR–GO/rGO).

deterioration of the network structures as temperature proceeded. The NBR–GO-1 showed very sharp decreasing trend after 170°C relative to others. This may be linked to the extensive oxidation process [1, 44] caused by the high O/C content present in GO. This facilitated the network deterioration at higher temperatures.

4.5.2. Reinforcement and Network Density Indices. The reinforcing factor (R_f) calculated from the fractional change in torque between the maximum torque of the composites, M_H (comp) and that of the gum, M_H (gum) for the various non-activated compounds was estimated using the Equation (13) and presented together in Figures 10(a), 10(b), 10(c), and 10(d).

$$R_f = \frac{M_{H(comp)} - M_{H(gum)}}{M_{H(gum)}}. \quad (13)$$

The increase in the mechanical strength index (M_H) from the rheometer is due to the higher network density index ($\Delta M = M_H - M_L$) for the composites at 160–190°C, relative to the gum shown in Figures 10(a) and 10(b). The role of the GO, rGO, and GRT within the matrix as

Table 4: The E_a (kJ/mol) of the un-activated sulfur cured systems by DSC.

Samples	Ozawa method, E_a (kJ/mol)		Kissinger method, E_a (kJ/mol)	
	Exothermic cure temperature (K)			
	T_{iv}	T_{fv}	T_{iv}	T_{fv}
NBR	82.15	93.23	75.62	86.11
NBR–GO-1	79.70	103.60	73.15	96.48
NBR–rGO-1	62.77	100.30	54.81	93.17

reinforcing fillers is computed as reinforcing factor (R_f) as shown in the plots Figures 10(c) and 10(d) for small and high filler content, respectively. Reinforcement of rubber matrix is known to depend on several factors, such as homogeneous dispersions of fillers, strong filler–filler, and filler–rubber interactions [64, 65].

Currently, the trend of increasing of the reinforcement (NBR–GRT > NBR–rGO > NBR–GO) follows the order of increasing of the O/C ratio (oxygenated groups on the fillers) given by (GRT > rGO > GO). Thus, the reinforcing action of these fillers may be dominated by stronger filler–rubber networks structures within the bulk matrix, owing to the oxygenated groups: epoxide (–C–O–C–), carboxyl (–O–C=O), and hydroxyl (–OH) [1]. Clearly, the absence of the ZnO/SA did not have any influence on the reinforcement of the NBR matrix.

It is fascinating to observe that, by increasing the ZnO/SA fraction from 0 (0 phr ZnO/0 phr SA) as in Figure 10(d) to 1 : 1(1 phr ZnO/1 phr SA) and 3.3 : 1.0 (5 phr ZnO/1.5 phr SA) ratios, the reinforcement factor dropped to 0.0124 for NBR–GO-1 and 0.0252 for NBR–GRT-1 in case of 1 : 1(ZnO/SA), and 0.0821 for NBR–GO-1 and 0.0412 for NBR–GRT-1 for the case of 3.3 : 1.0 (ZnO/SA), respectively.

Thus, high content of ZnO/SA in the rubber compounds favored reinforcing action, especially for the highly oxygenated filler (GO), despite the delays observed in vulcanization reaction. The current result shows higher torque properties compared with NBR–GNP-1 and NBR–carbon black (15–30 phr), which were prepared with all the curing ingredient (ZnO/SA, CZ/TMTD, and S), reported by Innes et al. [66]. This indicates the effectiveness of solution processing method in dispersions of GO or rGO fillers within rubber matrix compared with melt mixing methods [1].

4.6. Crosslinking Density Using Equilibrium Swelling. To understand the nature of reinforcement action of GO and rGO in NBR in the absence of ZnO/SA, the total crosslinking density, n_t (mol cm^{-3}) from the Young's modulus relation in Equation (9), the chemical network density, n_c (mol cm^{-3}) due to equilibrium swelling from Flory–Rhener Equation (11) and the differences, $n_p = n_t - n_c$ (mol cm^{-3}) are given in Table 5.

From Table 5, it can be realized that the NBR–GO compounds exhibit higher n_c at 0.1–1 phr of filler loading than NBR–rGO composites for compositions without ZnO/SA and those with reduced ratio of ZnO/SA (1 phr ZnO and 1 phr SA). This present result is in accordance with those compared between SBR–GO and SBR–rGO composites by Raef et al. [59], but relatively higher than those reported for XNBR reinforced with 1–5 phr of few layers of graphene composites, reported by Krishnan et al. [67], prepared with all the curing ingredients including ZnO/SA.

On close examination, the difference in n_c and n_t indicates that there may be a lot more physical interactions (n_p) in the NBR–GO composites than NBR–rGO. Meanwhile, NBR–rGO compounds dominates NBR–GO in terms of chemical networks (n_c) for the compounds prepared without TMTD reported by Mensah et al. [32] and those containing standard curing ingredient (5 phr of ZnO and 1.5 phr SA including 0.25 phr TMTD) collected from the previous work reported by Mensah et al. [35].

In addition, a careful comparison for the different compositions indicates that, low filler (0.1 phr) promotes low physical networks (n_p), whereas high filler content promotes high physical networks (n_p), in case of the traditional compositions (ZnO, SA, TMTD, CZ, and S) [35, 44]. Relatively, in case of the compounds prepared without ZnO/SA, 0.1 or 1 phr filler loading leads to high physical network density (n_p) by comparing with the traditional formulations.

In general, the incorporation of the fillers (~0.1–1 phr of GO, rGO, or GRT) into the NBR increased the total network density (n_t) including physical (n_p) and chemical networks (n_c). The increments of these properties with reference to the pure NBR matrix are expressed as percentages in brackets in Table 3. This increment may be due to proper dispersions of the fillers and their effective interactions with NBR chains.

According to Allahbakhsh et al. [43], increment in crosslink densities in composites is associated with reduction in free volume and solvent permeability [43]. Therefore, lower values of the solvent swelling degree (Q_r) with high reinforcement factor Q_R (Q_r/Q_m) was recorded for the composites. It is interesting to observe that GO, rGO, or GRT in the present compositions without ZnO/SA, or with low ratio of ZnO/SA (1 : 1) and those without TMTD [32], all exhibited high reinforcing role in NBR matrix than those which contain all the curing ingredients (ZnO, SA, TMTD, CZ, and S) [44].

In addition, at 1 phr filler loading, the present compositions example: NBR–GO-1 prepared without ZnO/SA and with reduced ZnO/SA exhibited significant improvement in the network density (n_c; 33% and 138%, respectively), in relation to the pure NBR. However, the network density (n_c) for NR–graphene sheets (1 phr) obtained 17% development in network density (n_c) relative to the pure NR [33].

It can therefore be suggested that proper dispersions of the graphene sheets decorated with desired oxygen–carbon ratio, may promote stronger filler–rubber interactions in a more polar matrix and in the presence of optimized amount of the cure ingredients (ZnO/SA, TMTD/CZ, and S) [35]. The results may be the reduction of the cure time without compromising with the other properties of the final composites.

4.7. Tensile Properties. Representative plots of stress against strain for sulfur cross-linked NBR and composites (NBR–

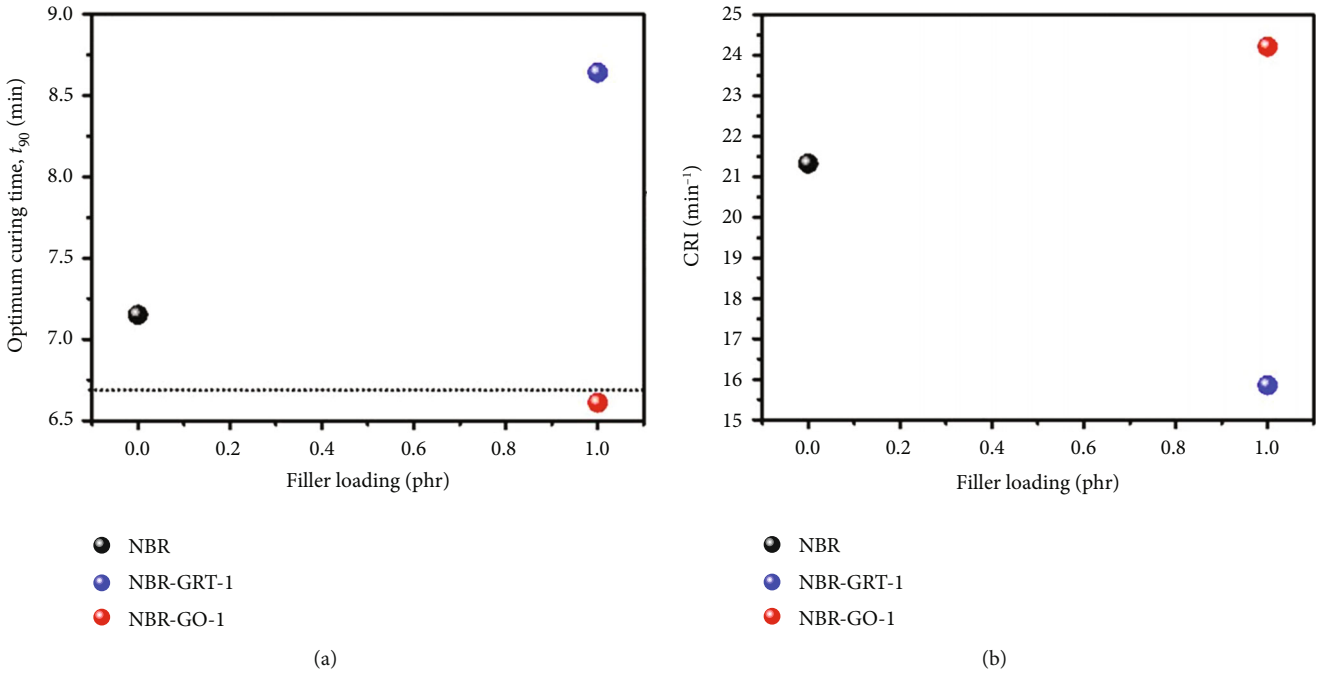

Figure 8: Cure rheometer characteristics of NBR–GO-1, NBR, and NBR–GRT-1 with optimized ZnO/SA ratio. (a) It is the cure time (t_{90}/minutes). (b) CRI (minutes^{-1}).

rGO and NBR–GO) prepared without ZnO/SA and those without TMTD are shown in Figures 11(a) and 11(b), respectively. The tensile properties including ultimate tensile strength (UTS, MPa), which is a measure of resistance to breaking of total networks, the stiffness or Young's modulus, E (MPa), the reinforcement ratio ($R_f = E_c/E_m$), and the elongation at break, E_{BR} (%) of the present compositions are matched with compositions with varied processing ingredients in Table 6.

It is evident from Figures 11(a) and 11(b) and Table 6, that incorporation of the GO/rGO/GRT into NBR generally raises the tensile properties (UTS (MPa) and E (MPa)) compared with neat NBR rubber, clearly at high filler loading. The efficiency of this development is expressed in % in the brackets in Table 6. The reinforcement strength can be seen in the high values of $R_f = E_c/E_m$ for the composites. The reinforcement mechanism responsible for this significant enhancement may be the effective distribution of reinforcements and the strong filler–rubber bonding in the various compositions [9, 10, 12, 32] measured by the low equilibrium swelling degree (Q_r) and high network densities created (refer to Table 5), especially between the highly oxygenated graphene sheets (GO and rGO) with and the main matrix.

In the previous report by Mensah et al. [35, 44], it was observed that the UTM (MPa) and E_{BR} (%) for NBR–rGO was inferior compared with NBR–GO compounds for the standard composition containing all ingredients (ZnO/SA, CZ/TMTD, and S) shown in composition *d*. The order for the decrease in UTM (MPa) and the E_{BR} (%) can be respectively written as: NBR–GO-0.1 > NBR–GO-1 > NBR–rGO-0.1 > NBR–rGO-1 > NBR and NBR–GO-0.1 > NBR–GO-1 > NBR > NBR–rGO-1 > NBR–rGO-0.1.

On close inspection, when the activator ZnO/SA was removed (composition *a*) or reduced (ZnO/SA) to a ratio of 1 in the compounds (composition *b*), NBR–GO still obtained higher tensile properties (UTM (MPa), E (MPa), R_f and E_{BR} (%)) than NBR–rGO composites. Typically, the order of decreasing trend for the UTM (MPa) and the E_{BR} (%) can be, respectively, written as: NBR–GO-1 > NBR–rGO-1 > NBR–GO-0.1 > NBR–rGO-0.1 > NBR and NBR–GO-1 > NBR–rGO-1 > NBR > NBR–GO-0.1 > NBR–rGO-0.1. This suggests that GO still formed adequate bonding with the NBR matrix than rGO, by the help of the many oxygen groups: carboxyl (–O–C=O), epoxide (–C–O–C–), and hydroxyl (–OH), which perhaps played self-activator role during crosslinking process [44]. This observation is in correspondence with the M_H properties discussed above.

On the other hand, it was fascinating to also have observed that, NBR–rGO composites generally recorded higher tensile strength (UTM (MPa) and E_{BR} (%) than NBR–GO, but showed close correlation in E (MPa) and R_f) properties with NBR–GO, on exclusion of TMTD from the composition (*c*) recently stated by Mensah et al. [32]. The decreasing trend for the UTM (MPa) and E_{BR} (%) was written as: NBR–rGO-1 > NBR–rGO-0.1 > NBR–GO-0.1 > NBR–GO-1 > NBR and NBR–rGO-0.1 > NBR–GO-0.1 > NBR–rGO-1 > NBR > NBR–GO-1, respectively.

Again, the NBR–rGO composites exhibited relatively higher stiffness compared with NBR–GO compounds. The drop in UTM (MPa) and lower stiffness recorded for compared with NBR–rGO and NBR–GO compounds when TMTD was removed from the composition was ascribed to poor chemical crosslink density n_c (mol cm^{-3}) formation in NBR–GO (see Table 5) [32]. It was consequently observed that the self-acceleration role of the fillers (GO and rGO)

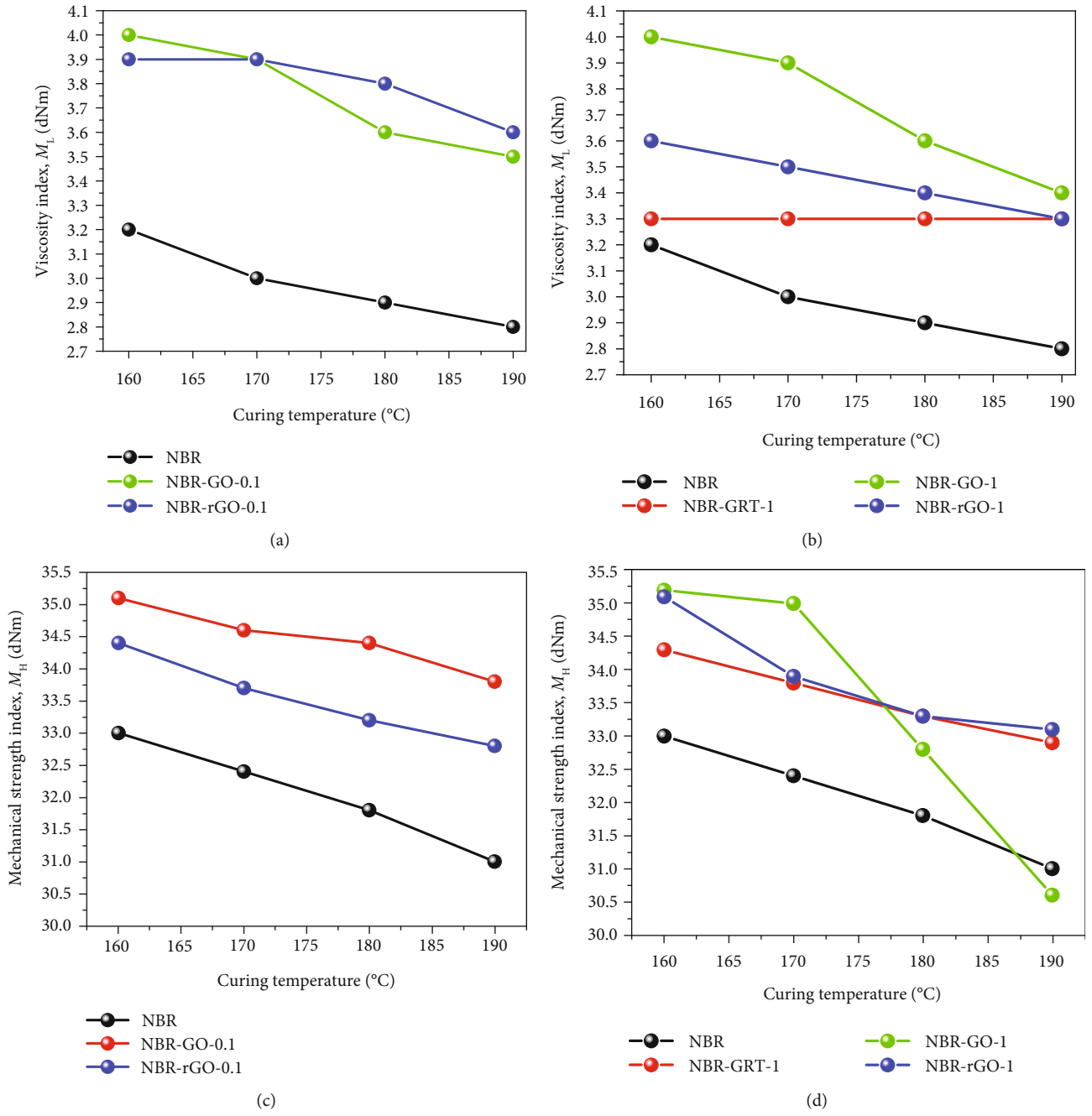

Figure 9: Mechanical strength index and viscosity index from the rheometer. (a) Viscosity index (M_L) of 0.1 phr filled compounds. (b) Viscosity index (M_L) of 1 phr filled compounds. (c) Mechanical strength index (M_H) of 0.1 phr filled compounds. (d) Mechanical strength index (M_H) of 1 phr filled compounds.

was noted to also depend on successful dispersions of the fillers within the matrix. This was seen with the lower equilibrium swelling degree (Q_r) recorded for the NBR–GO and NBR–rGO compounds compared with NBR (Table 5). The lower Q_r values has been widely used to justify effectiveness of filler dispersions within in rubber and/or high filler–rubber interactions [50, 68, 69].

Hence, it is not a surprised to see the composites exhibiting effective self-activation role in the absence of ZnO/SA compared with gum (NBR) in terms of the tensile properties recorded. Consequently, even in the absence of the ZnO/SA, the present composition (NBR–GO-1 and NBR–rGO-1) has exhibited higher UTM properties than NBR reinforced with 1 phr of graphene nanoplatelets compounded with standard cure ingredients (ZnO/SA, CZ/TMTD, and S), reported recently by Innes et al. [66].

Clearly, from Table 5, when the standard compositions (*d*) [35, 44] are compared in terms of UTM (MPa), especially for the highly loaded (1 phr GO) samples, a drop of over 56% and 17% were recorded when TMTD (composition *c*) [32] and ZnO/SA (composition *a*) were removed. In comparison,

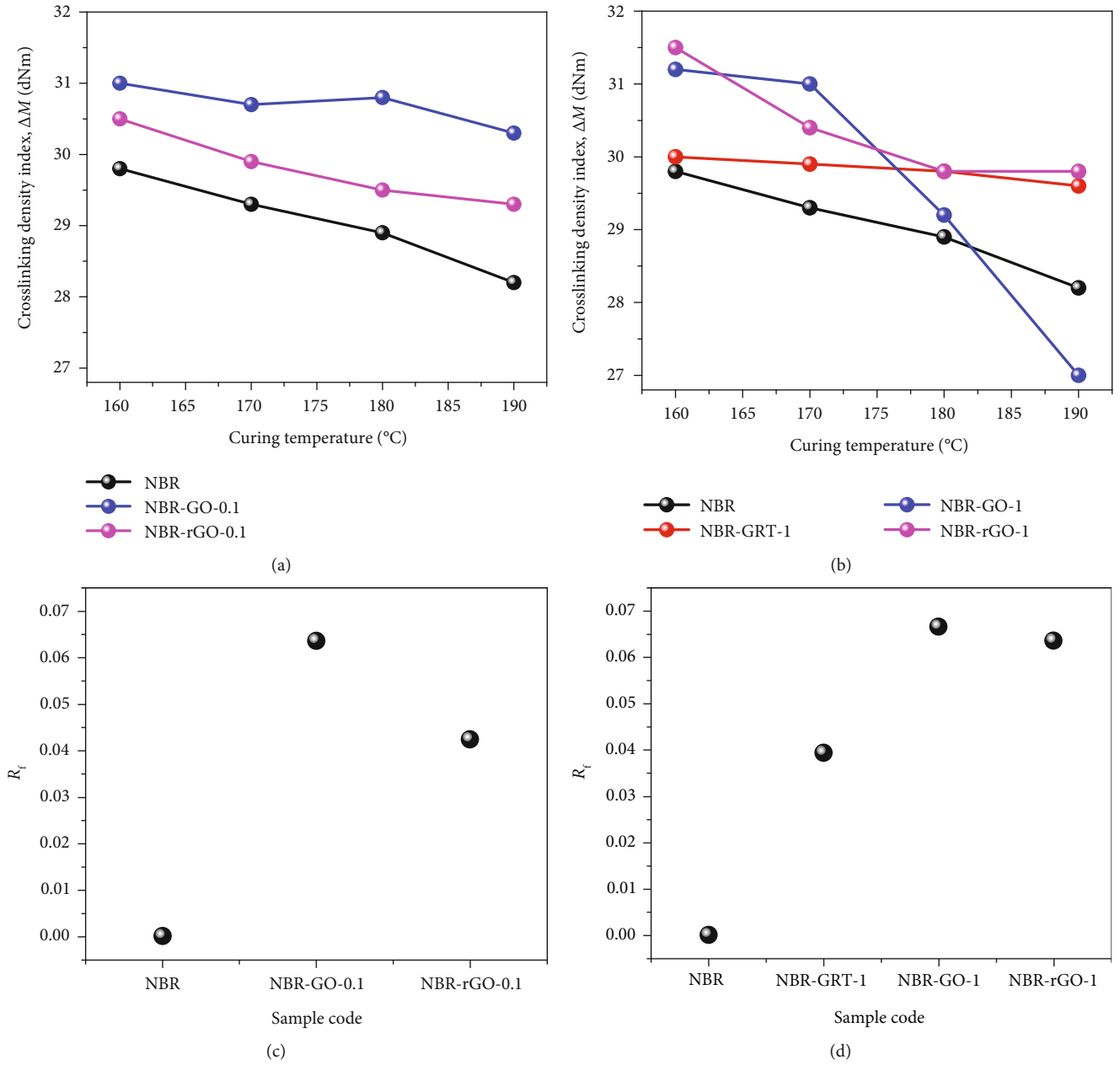

Figure 10: Network density from cure rheology: (a) at 0.1 phr filled compounds, (b) at 1 phr filled compounds and reinforcing factor for (c) 0.1 phr filled compounds, and (d) 1 phr filled compounds.

NBR–rGO-1 showed almost no change in UTM (MPa) when TMTD was removed and a drop of ~9% when the ZnO/SA was absent from the present composition.

On account of crosslinking density, n_c (mol cm^{-3}; Table 6), composition (*a*) recorded a drop of 72% and 58% relative to those without TMTD and ZnO/SA, respectively. Interestingly, that of NBR–rGO-1 recorded a drop of over 163% and 190% in n_c (mol cm^{-3}) when compared with those in composition (*c*) in Mensah et al. [32], work and composition (*a*) for the present work.

It can therefore be concluded that when TMTD and ZnO/SA were removed from the NBR–GO/rGO, the UTM (MPa) behavior of NBR–GO systems relied mainly on the presence of complete and stable crosslinks formation (NBR–S_x–GO). However, the moderate drops in the values of UTM (MPa) observed for the NBR–rGO compounds may be due to the combined effect of the higher concentration of physical networks (rGO–rGO or rGO–S_x–rGO) in addition to the presence of desired chemical links (NBR–S_x–rGO), since the UTM (MPa) property is generally a collective effect of physical and chemical network densities/interactions [1, 10].

5. Conclusion

The impact of un-activated sulfur vulcanized NBR, NBR–rGO, and NBR–GO was carefully investigated. The

Table 5: Swelling and crosslinking density of samples.

Samples	Q_r	Q_R (Q_r/Q_m)	n_c ($\times10^{-3}$)	n_t ($\times10^{-3}$)	n_p [$n_t - n_c$] ($\times10^{-3}$)
NBR[a]	2.6	1	0.9 (—)	1.39 (—)	0.49 (—)
NBR–GO-0.1[a]	2.56	0.98	1 (11%)	2.54 (83%)	1.54 (214%)
NBR–GO-1[a]	2.4	0.92	1.2 (33%)	2.79 (101%)	1.59 (224%)
NBR–rGO-0.1[a]	2.51	0.97	1 (11%)	2.08 (50%)	1.08 (120%)
NBR–rGO-1[a]	2.49	0.96	1 (11%)	2.64 (90%)	1.64 (235%)
NBR[b]	3.21	1	0.6 (—)	—	—
NBR–GO-1[b]	2.09	0.65	1.7 (183%)	—	—
NBR–GRT-1[b]	2.76	0.86	0.9 (50%)	—	—
NBR[c]	2.6	1	0.9 (—)	1.28 (—)	0.36 (—)
NBR–GO-1[c]	2.5	0.96	1 (11%)	2.52 (97%)	1.52 (322%)
NBR–rGO-1[c]	2.45	0.94	1.1 (22%)	2.42 (89%)	1.32 (267%)
NBR[d]	2.30	1	1.3 (—)	1.39 (—)	0.4 (—)
NBR–GO-0.1[d]	2.20	0.96	1.5 (15 %)	1.94 (40%)	0.44 (10%)
NBR–GO-1[d]	1.90	0.96	1.9 (46 %)	2.5 (80%)	1.5 (275%)
NBR–rGO-0.1[d]	2.12	0.95	1.5 (15 %)	2.26 (63%)	0.76 (90%)
NBR–rGO-1[d]	1.8	0.96	2.9 (123%)	2.4 (73%)	1.3 (225%)

Q_r: swelling degree; Q_o and Q_R: equilibrium swelling ratio of the filled and unfilled elastomer; n_c: chemical crosslinking density; n_t: total network density; n_p: physical crosslinks. [a]Current compounds with 0 phr of ZnO/SA. [b]Compounds with 1 phr of ZnO/1 phr of SA. [c]Compounds without TMTD [32]. [d]Compounds with traditional processing ingredient (5 phr of ZnO and 1.5 phr SA including 0.25 phr TMTD) [44].

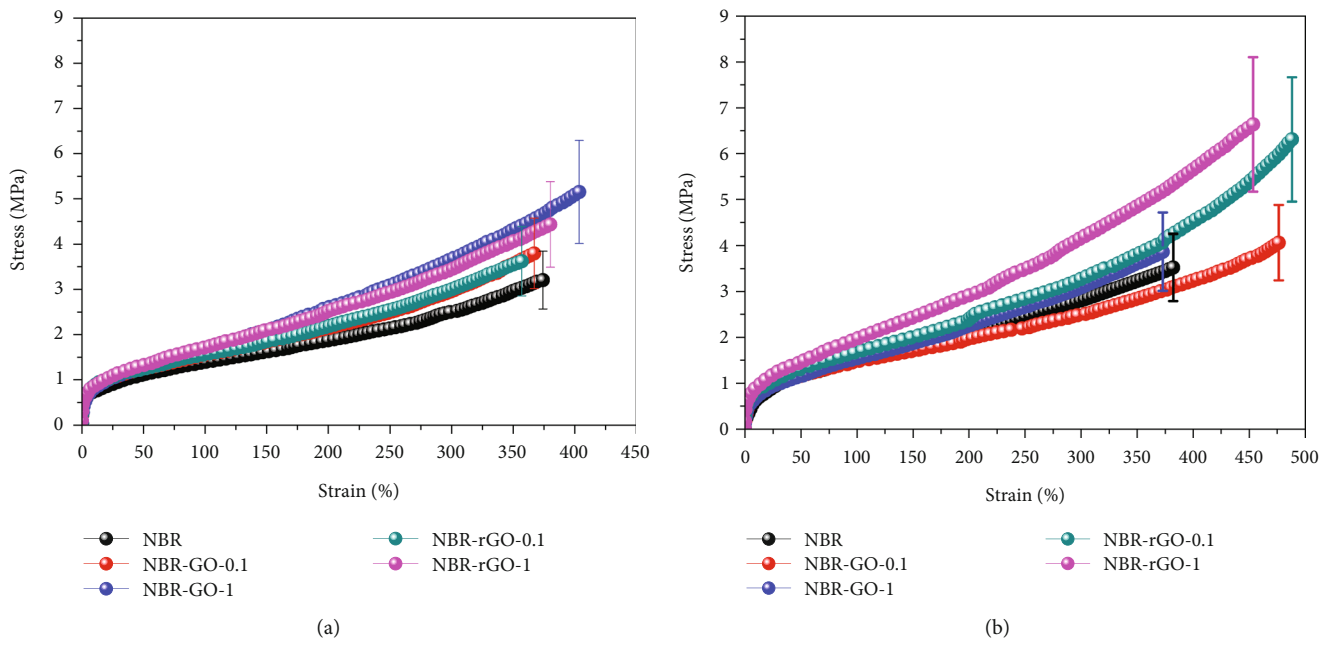

Figure 11: Representatives stress–strain curves for NBR and the filled compounds: (a) Compounds prepared without ZnO/SA. (b) Compounds prepared without TMTD [32].

rheometric cure analysis showed strong relationship in CRI among the entire compounds. Generally, NBR cured relatively faster than the composites. This was seen in the lower E_a (kJ/mol) measured using autocatalytic, Ozawa and Kissinger methods. The reason for the delays in curing the composites was assigned to the incorporated GO/rGO sheets and the absence of ZnO/SA to activate the vulcanization process. NBR–rGO showed relatively faster curing behavior than the NBR–GO composites, especially at higher filler content (1 phr). This was linked to the activator role played by the high oxygen (–O–C=O, C–O, and O–H) content on the surface of rGO particles, assisted by the effective dispersions within NBR. Regardless of the delay in curing, the composites broadly obtained high viscosity (M_L) and crosslinking density indicator (ΔM) than NBR, with NBR–GO taking the lead. The enhancements in (M_L and ΔM) of the NBR–GO

Table 6: Tensile properties of CZ-accelerated NBR–GDS vulcanizates.

Sample code	UTM (MPa)	E (MPa)	$R_f = E_c/E_m$	E_{BR} (%)
NBR[a]	3.2 (—)	9.5 (—)	1	374 (—)
NBR–GO-0.1[a]	3.8 (18.8%)	17.3 (82.1%)	1.8	367 (−1.9%)
NBR–GO-1[a]	5.2 (62.5%)	19.0 (100%)	2	404 (8.0%)
NBR–rGO-0.1[a]	3.6 (12.5%)	14.1 (48.4%)	1.5	357 (−4.8)
NBR–rGO-1[a]	4.4 (37.5%)	18.0 (89.5%)	1.9	380 (1.6%)
NBR[b]	4.2 (—)	—	—	420 (—)
NBR–GO-1[b]	5.5 (31%)	—	—	460 (9.5%)
NBR–GRT-1[b]	4.7 (11.9%)	—	—	420 (0.0%)
NBR–rGO-1[b]	4.9 (16.7%)	—	—	400 (−5%)
NBR[c]	3.5 (—)	8.7 (—)	1	382 (—)
NBR–GO-0.1[c]	4.1 (17.1%)	12.1 (39.1%)	1.4	476 (24.6%)
NBR–GO-1[c]	3.9 (11.4%)	17.2 (97.7%)	2.0	373 (−2.4%)
NBR–rGO-0.1[c]	6.3 (80%)	12.0 (37.9%)	1.4	488 (27.8%)
NBR–rGO-1[c]	6.6 (88.5%)	16.5 (89.7%)	1.9	454 (18.9%)
NBR[d]	4.0 (—)	3.9 (—)	1	337 (—)
NBR–GO-0.1[d]	7.7 (92.5%)	13.2 (238.5)	3.4	567 (68.2%)
NBR–GO-1[d]	6.1 (52.5%)	19.7 (405.1%)	5.1	454 (34.7%)
NBR–rGO-0.1[d]	5.7 (42.5%)	15.4 (294.9%)	4.0	241 (−39.8%)
NBR–rGO-1[d]	4.8 (20%)	22.2 (469.2%)	5.7	336 (−0.3%)

UTS: ultimate tensile strength (MPa); E: Young's modulus (MPa); EBR (%), elongation at break. [a]Current compounds with 0 phr of ZnO/SA. [b]Compounds with 1 phr of ZnO/1 phr of SA. [c]Compounds with without TMTD [32]. [d]Standard or compounds with traditional processing ingredient (5 phr of ZnO and 1.5 phr SA including 0.25 phr TMTD) [35, 44].

composites was also revealed in the mechanical properties (UTS (MPa), elongation break E_{BR} (%), chemical network n_c (mol cm^{-3}), and total network n_t (mol cm^{-3}) density evaluations). The results in this current study suggest that exclusion of ZnO/SA from NBR compounds may somehow affect the curing speed of the NBR–GO/rGO composites and could also decrease their network density, compared with those containing ZnO/SA. Interestingly, when the ratio of ZnO/SA (1.33 : 1) was reduced to 1 : 1, even the highly oxygenated graphene (GO) cured faster than NBR. Therefore, the future prospects of NBR–GO/rGO based composites will depend strongly on several factors, including the optimization of ZnO/SA and CZ/TMTD in the composition design, by using desired rubber matrix, and understanding of the size, type, and chemical functionalities of GDS. This include being able to successfully quantify the amount of oxygen moieties (–O–C=O, –C–O–C–, and –OH) attached to GDS for effective network formation with the matrix. These factors may help to unravel some of the curing mysteries of rubber–GDS, which influences their physico-mechanical properties for future applications in developing rubber–GDS materials for gaskets, O-rings, automobile parts, and sensors. Finally, future studies on the effect of wrinkled GDS on curing of rubber matrix using TEM, will be necessary to fully understand the mechanical interlocking effects in chain-wrinkled GDS composites.

Data Availability

Data supporting this research article are available from the corresponding author or first author on reasonable request.

Consent

The corresponding author has consent from all co-authors.

Conflicts of Interest

The author(s) declare(s) that they have no conflicts of interest.

Authors' Contributions

The author (Dr. Bismark Mensah) is responsible for design and funding of experiment. Bismark Mensah carried out the entire experiment, data analysis, drafting, and revision of manuscript. The authors (Prof. Boateng Onwona-Agyeman, Prof. Johnson Efavi Kwame, Dr. Frank Nsaful, and Dr. Daniel Akwei Addo) contributed in data analysis and revision of the manuscript. The other authors (Ralph Abakah Ofori, Mawufemor Zigah, Joyce Koranteng, and Maxwell Karikari) also contributed in revision of the manuscript.

Acknowledgments

We gratefully acknowledge Prof. Changwoon Nah of the Polymer Engineering Department, JBNU (South Korea) for giving us the permission to conduct this research at their facility. We again thank the University of Ghana—Carnegie Next Generation of African Academics (UG-Carnegie-BANGA) Project and the University of Ghana's Office of Research Innovation and Development (ORID) for their assistance in completing the manuscript. Self funding.

References

[1] B. Mensah, K. C. Gupta, H. Kim et al., "Graphene-reinforced elastomeric nanocomposites: a review," *Polymer Testing*, vol. 68, pp. 160–184, 2018.

[2] A. Das, D.-Y. Wang, K. W. Stöckelhuber et al., "Rubber–clay nanocomposites: some recent results," in *Advanced Rubber Composites*, G. Heinrich, Ed., pp. 85–166, Springer, Berlin, Heidelberg, 2010.

[3] S. Salaeh, G. Boiteux, P. Cassagnau et al., "Conductive elastomer composites with low percolation threshold based on carbon black and epoxidized natural rubber," *Polymer Composites*, vol. 39, pp. 1835–1844, 2018.

[4] Z.-Y. Li, Y.-H. Song, and Q. Zheng, "Payne effect and weak overshoot in rubber nanocomposites," *Chinese Journal of Polymer Science*, vol. 40, pp. 85–92, 2022.

[5] W. Liu, L. Lv, Z. Yang et al., "The effect of OMMT on the properties of vehicle damping carbon black-natural rubber composites," *Polymers*, vol. 12, p. 1983, 2020.

[6] M. Hernández, M. M. Bernal, R. Verdejo et al., "Overall performance of natural rubber/graphene nanocomposites," *Composites Science and Technology*, vol. 73, pp. 40–46, 2012.

[7] X. Liu, L.-Y. Wang, L.-F. Zhao et al., "Research progress of graphene-based rubber nanocomposites," *Polymer Composites*, vol. 39, pp. 1006–1022, 2016.

[8] B. Mensah, D. S. Konadu, and B. Agyei-Tuffour, "Effects of graphene oxide and reduced graphene oxide on the mechanical and dielectric properties of acrylonitrile-butadiene rubber and ethylene-propylene-diene-monomer blend," *International Journal of Polymer Science*, vol. 2022, 2022.

[9] B. Mensah and E. Oduro, "Preparation and characterization of hydrophilic and water-swellable elastomeric nanocomposites," *Polymer Engineering & Science*, vol. 63, pp. 738–754, 2023.

[10] B. Mensah, B. Onwona-Agyeman, E. Nyankson et al., "Effect of palm oil as plasticizer for compounding polar and nonpolar rubber matrix reinforced carbon black composites," *Journal of Polymer Research*, vol. 30, p. 67, 2023.

[11] A. K. Hussain, I. Sudin, U. M. Basheer et al., "A review on graphene-based polymer composite coatings for the corrosion protection of metals," *Corrosion Reviews*, vol. 37, pp. 343–363, 2019.

[12] B. Mensah, A. Yaya, B. Onwona-Agyeman et al., "A study of the interactions of carbon based fillers in acrylonitrile butadiene rubber matrix for high deformation sensor applications," *Journal of Reinforced Plastics and Composites*, vol. 2023, pp. 1–16, 2023.

[13] T. Wei, G. Luo, Z. Fan et al., "Preparation of graphene nanosheet/polymer composites using in situ reduction-extractive dispersion," *Carbon*, vol. 47, pp. 2296–2299, 2009.

[14] A. Sethulekshmi, J. S. Jayan, A. Saritha et al., "Recent developments in natural rubber nanocomposites containing graphene derivatives and its hybrids," *Industrial Crops and Products*, vol. 177, p. 114529, 2022.

[15] T. D. Dao, H. I. Lee, and H. M. Jeong, "Alumina-coated graphene nanosheet and its composite of acrylic rubber," *Journal of Colloid and Interface Science*, vol. 416, pp. 38–43, 2014.

[16] X. Xiong, J. Wang, H. Jia et al., "Structure, thermal conductivity, and thermal stability of bromobutyl rubber nanocomposites with ionic liquid modified graphene oxide," *Polymer Degradation and Stability*, vol. 98, pp. 2208–2214, 2013.

[17] X. Duan, R. Tao, Y. Chen et al., "Improved mechanical, thermal conductivity and low heat build-up properties of natural rubber composites with nano-sulfur modified graphene oxide/silicon carbide," *Ceramics International*, vol. 48, pp. 22094–22104, 2022.

[18] S.-H. Bae, Y. Lee, B. K. Sharma et al., "Graphene-based transparent strain sensor," *Carbon*, vol. 51, pp. 236–242, 2013.

[19] C. S. Boland, U. Khan, C. Backes et al., "Sensitive, high-strain, high-rate bodily motion sensors based on graphene-rubber composites," *ACS Nano*, vol. 8, pp. 8819–8830, 2014, 2014/08/08.

[20] F. Shahzad, S. Yu, P. Kumar et al., "Sulfur doped graphene/polystyrene nanocomposites for electromagnetic interference shielding," *Composite Structures*, vol. 133, pp. 1267–1275, 2015.

[21] J. J. Edayadiyil, J. Abraham, S. Rajeevan et al., "Synthesis and characterization of natural rubber/graphene quantum dot nanocomposites," *Journal of Polymer Research*, vol. 28, pp. 1–8, 2021.

[22] B. Chen, J. Dai, T. Song et al., "Research and development of high-performance high-damping rubber materials for high-damping rubber isolation bearings: a review," *Polymers*, vol. 14, p. 2427, 2022.

[23] M. Porter, "Rubber Technology Handbook," *British Polymer Journal*, vol. 23, pp. 359–359, 1990, Rubber Technology Handbook Werner Hofmann, Carl Hanser Verlag, Munich, 1989. pp. xv + 611, price dm 86.00. isbn 3–446–14895–7.

[24] M. Moniruzzaman and K. I. Winey, "Polymer nanocomposites containing carbon nanotubes," *Macromolecules*, vol. 39, pp. 5194–5205, 2006.

[25] E. T. Thostenson, Z. F. Ren, and T. W. Chou, "Advances in the science and technology of carbon nanotubes and their composites: a review," *Composites Science and Technology*, vol. 61, pp. 1899–1912, 2001.

[26] D. Choi, M. A. Kader, B.-H. Cho et al., "Vulcanization kinetics of nitrile rubber/layered clay nanocomposites," *Journal of Applied Polymer Science*, vol. 98, pp. 1688–1696, 2005.

[27] M. Akiba and A. S. Hashim, "Vulcanization and crosslinking in elastomers," *Progress in Polymer Science*, vol. 22, pp. 475–521, 1997.

[28] A. Coran and J. Eirich, "7 Vulcanization," *Science and Technology of Rubber*, pp. 339–385, 1994.

[29] S.-M. Kim and K.-J. Kim, "Effects of accelerators on the vulcanization properties of silica vs. carbon black filled natural rubber compounds," *Polymer Korea*, vol. 37, pp. 269–275, 2013.

[30] P. Ghosh, S. Katare, P. Patkar et al., "Sulfur vulcanization of natural rubber for benzothiazole accelerated formulations: from reaction mechanisms to a rational kinetic model," *Rubber Chemistry and Technology*, vol. 76, pp. 592–693, 2003.

[31] G. Heideman, R. N. Datta, J. W. M. Noordermeer et al., "Influence of zinc oxide during different stages of sulfur vulcanization. Elucidated by model compound studies," *Journal of Applied Polymer Science*, vol. 95, pp. 1388–1404, 2005.

[32] B. Mensah, Y. D. Bensah, P. S. F. Nbelayim et al., "Vulcanization kinetics of acrylonitrile-butadiene rubber reinforced with graphene oxide and reduced graphene oxide in the absence of co-cure accelerator," *Polymer Engineering & Science*, vol. 62, pp. 4156–4172, 2022.

[33] J. Wu, W. Xing, G. Huang et al., "Vulcanization kinetics of graphene/natural rubber nanocomposites," *Polymer*, vol. 54, pp. 3314–3323, 2013.

[34] M. Barghamadi, M. Karrabi, M. H. R. Ghoreishy et al., "Effects of two types of nanoparticles on the cure, rheological, and mechanical properties of rubber nanocomposites based on

the NBR/PVC blends," *Journal of Applied Polymer Science*, vol. 136, p. 47550, 2019.

[35] B. Mensah, S. I. Kang, W. Wang et al., "Effect of graphene on polar and nonpolar rubber matrices," *Mechanics of Advanced Materials and Modern Processes*, vol. 4, p. 1, 2018.

[36] B. Mensah, S. Kim, S. Arepalli et al., "A study of graphene oxide-reinforced rubber nanocomposite," *Journal of Applied Polymer Science*, vol. 131, pp. 40640–40671, 2014.

[37] H. E. Kissinger, "Reaction kinetics in differential thermal analysis," *Analytical Chemistry*, vol. 29, pp. 1702–1706, 1957.

[38] T. Ozawa, "A new method of analyzing thermogravimetric data," *Bulletin of the Chemical Society of Japan*, vol. 38, pp. 1881–1886, 1965.

[39] T. V. Varghese, H. Ajith Kumar, S. Anitha et al., "Reinforcement of acrylonitrile butadiene rubber using pristine few layer graphene and its hybrid fillers," *Carbon*, vol. 61, pp. 476–486, 2013.

[40] A. De Falco, A. J. Marzocca, M. A. Corcuera et al., "Accelerator adsorption onto carbon nanotubes surface affects the vulcanization process of styrene-butadiene rubber composites," *Journal of Applied Polymer Science*, vol. 113, pp. 2851–2857, 2009.

[41] G. Mathew, J. M. Rhee, Y. S. Lee et al., "Cure kinetics of ethylene acrylate rubber/clay nanocomposites," *Journal of Industrial and Engineering Chemistry*, vol. 14, pp. 60–65, 2008.

[42] M. J. Azizli, M. Mokhtary, H. A. Khonakdar et al., "Compatibilizer/graphene/carboxylated acrylonitrile butadiene rubber (XNBR)/ethylenepropylenediene monomer (EPDM) nanocomposites: morphology, compatibility, rheology and mechanical properties," *Journal of Applied Polymer Science*, vol. 137, p. app49331, 2020.

[43] A. Allahbakhsh, S. Mazinani, M. R. Kalaee et al., "Cure kinetics and chemorheology of EPDM/graphene oxide nanocomposites," *Thermochimica Acta*, vol. 563, pp. 22–32, 2013.

[44] B. Mensah, K. C. Gupta, G. Kang et al., "A comparative study on vulcanization behavior of acrylonitrile-butadiene rubber reinforced with graphene oxide and reduced graphene oxide as fillers," *Polymer Testing*, vol. 76, pp. 127–137, 2019.

[45] B. Mensah, D. Kumar, D.-K. Lim et al., "Preparation and properties of acrylonitrile–butadiene rubber–graphene nanocomposites," *Journal of Applied Polymer Science*, vol. 132, pp. 42457–42469, 2015.

[46] M. Barghamadi, M. H. R. Ghoreishy, M. Karrabi et al., "Investigation on the kinetics of cure reaction of acrylonitrile–butadiene rubber (NBR)/polyvinyl chloride (PVC)/graphene nanocomposite using various models," *Journal of Applied Polymer Science*, vol. 137, p. 48632, 2020.

[47] S. Montserrat and J. Málek, "A kinetic analysis of the curing reaction of an epoxy resin," *Thermochimica Acta*, vol. 228, pp. 47–60, 1993.

[48] B. Karaagac, M. Inal, and V. Deniz, "Predicting optimum cure time of rubber compounds by means of ANFIS," *Materials & Design*, vol. 35, pp. 833–838, 2012.

[49] H. J. Borchardt and F. Daniels, "The application of differential thermal analysis to the study of reaction kinetics," *Journal of the American Chemical Society*, vol. 79, pp. 41–46, 1957.

[50] P. J. Flory and J. Rehner, "Statistical mechanics of cross-linked polymer networks II. Swelling," *The Journal of Chemical Physics*, vol. 11, pp. 521–526, 1943.

[51] G. M. Bristow and W. F. Watson, "Cohesive energy densities of polymers. Part 1. Cohesive energy densities of rubbers by swelling measurements," *Transactions of the Faraday Society*, vol. 54, pp. 1731–1741, 1958.

[52] C. Nah, J. Y. Lim, R. Sengupta et al., "Slipping of carbon nanotubes in a rubber matrix," *Polymer International*, vol. 60, pp. 42–44, 2011.

[53] H. Kang, Y. Tang, L. Yao et al., "Fabrication of graphene/natural rubber nanocomposites with high dynamic properties through convenient mechanical mixing," *Composites Part B: Engineering*, vol. 112, pp. 1–7, 2017.

[54] N. Dehbari, J. Tavakoli, J. Zhao et al., "In situ formed internal water channels improving water swelling and mechanical properties of water swellable rubber composites," *Journal of Applied Polymer Science*, vol. 134, p. 44548, 2017.

[55] A. Das, D.-Y. Wang, K. W. Stoeckelhuber et al., "Rubber-clay nanocomposites: some recent results," *Advanced Rubber Composites*, G. Heinrich, Ed., pp. 85–166, Springer, Berlin, Heidelberg, 2011.

[56] C. Hayichelaeh and K. Boonkerd, "Enhancement of the properties of carbon-black-filled natural rubber compounds containing soybean oil cured with peroxide through the addition of coagents," *Industrial Crops and Products*, vol. 187, p. 115306, 2022.

[57] N. Moazeni, Z. Mohamad, and N. Dehbari, "Study of silane treatment on poly-lactic acid(PLA)/sepiolite nanocomposite thin films," *Journal of Applied Polymer Science*, vol. 132, p. 41428, 2015.

[58] X. Hu, H. Zhao, T. Li et al., "Acrylonitrile–butadiene rubber reinforced by graphene oxide/halloysite nanotubes hybrid nanofillers through mechanical blending method," *Plastics, Rubber and Composites*, vol. 49, pp. 141–149, 2020.

[59] M. Raef, S. M. Hosseini, M. Nabavian Kalat et al., "Vulcanization kinetics of styrene butadiene rubber reinforced by graphenic particles," *SPE Polymers*, vol. 2, pp. 122–133, 2021.

[60] M. A. Kader and C. Nah, "Influence of clay on the vulcanization kinetics of fluoroelastomer nanocomposites," *Polymer*, vol. 45, pp. 2237–2247, 2004.

[61] G. Sui, W. H. Zhong, X. P. Yang et al., "Curing kinetics and mechanical behavior of natural rubber reinforced with pretreated carbon nanotubes," *Materials Science and Engineering: A*, vol. 485, pp. 524–531, 2008.

[62] M. J. Azizli, M. Barghamadi, K. Rezaeeparto et al., "Theoretical and experimental analyses of rheological, compatibility and mechanical properties of PVMQ/XNBR-g GMA/XNBR/GO ternary hybrid nanocomposites," *Iranian Polymer Journal*, vol. 30, pp. 1001–1018, 2021.

[63] T. P. Selvin, J. Kuruvilla, and T. Sabu, "Mechanical properties of titanium dioxide-filled polystyrene microcomposites," *Materials Letters*, vol. 58, pp. 281–289, 2004.

[64] L. Bokobza, "The reinforcement of elastomeric networks by fillers," *Macromolecular Materials and Engineering*, vol. 289, pp. 607–621, 2004.

[65] S. Qian, J. Huang, W. Guo et al., "Investigation of carbon black network in natural rubber with different bound rubber contents," *Journal of Macromolecular Science Part B-Physics*, vol. 46, pp. 453–466, 2007.

[66] J. R. Innes, R. J. Young, and D. G. Papageorgiou, "Graphene nanoplatelets as a replacement for carbon black in rubber compounds," *Polymers*, vol. 14, p. 1204, 2022.

[67] S. Krishnan, G. M. Maya, A. Das et al., "In-situ interfacial compatibilization via edge-sulfurated few layer graphene during the formation of crosslinked graphene–rubber nanocomposites," *Scientific Reports*, vol. 12, p. 4013, 2022.

[68] K. Ahmed, S. S. Nizami, N. Z. Raza et al., "Mechanical, swelling, and thermal aging properties of marble sludge-natural rubber composites," *International Journal of Industrial Chemistry*, vol. 3, p. 21, 2012.

[69] B. Mensah, L. N. Damoah, E. Nyankson et al., "Effect of Shea butter as plasticizer on natural rubber-carbon black reinforced composites," *Journal of Elastomers and Plastics*, vol. 54, pp. 1238–1253, 2022.